THE NATURE AND DETERMINATION OF THE DYNAMIC GLASS TRANSITION TEMPERATURE IN POLYMERIC LIQUIDS

by

PAUL JOHN MLYNARCZYK

B.S., University of Illinois at Urbana-Champaign, 2008

M.S., North Carolina State University, 2011

A REPORT

Submitted in partial fulfillment of the requirements for the degree

MASTER OF SCIENCE

Department of Chemical Engineering
College of Engineering

KANSAS STATE UNIVERSITY
Manhattan, Kansas

2014

Approved by:

Major Professor
Dr. Jennifer L. Anthony

Abstract

A polymer has drastically different physical properties above versus below some characteristic temperature. For this reason, the precise identification of this glass transition temperature, T_g, is critical in evaluating product feasibility for a given application.

The objective of this report is to review the behavior of polymers near their T_g and assess the capability of predicting T_g using theoretical and empirical models. It was determined that all polymers begin to undergo structural relaxation at various temperatures both nearly above and below T_g, and that practical assessment of a single consistent T_g is successfully performed through consideration of only immediate thermal history and thermodynamic properties. It was found that the best quantitative structure-property relationship (QSPR) models accurately predict T_g of polymers of theoretically infinite chain length with an average error of less than 20 K or about 6%, while T_g prediction for shorter polymers must be done by supplementing these $T_g(\infty)$ values with configurational entropy or molecular weight relational models. These latter models were found to be reliable only for polymers of molecular weight greater than about 2,000 g/mol and possessing a $T_g(\infty)$ of less than about 400 K.

Table of Contents

List of Figures

List of Tables

Acknowledgments

This report was made possible through the instruction and assistance of the faculty and staff at Kansas State University. I would first like to thank Dr. Jennifer Anthony for her patience, support, and constructive feedback throughout the composition of this report. I would also like to recognize the other two supervisory committee members, Dr. Larry Glasgow and Dr. John Schlup. Much of the inspiration for this report came from concepts learned from courses taught by all three of these professors.

Introduction

The glass transition temperature, T_g, denotes the changeover point at which a material behaves like a glass or a rubber, and is among the most important characteristic values of a polymer. The drastic differences in physical and mechanical properties below versus above the T_g make its precise identification critical, and is thus one of the first values measured after synthesizing a new polymer. The T_g value will dictate the acceptable operating temperature range of a polymer for a desired application. In the context of synthesis of new polymer compounds, the T_g will determine the associated feasibility for the intended application. This report aims to evaluate the capability of current theoretical and empirical models to characterize and predict the T_g.

An illustration of the potential catastrophic consequences of oversight of appropriate operating temperature range can be seen in the infamous space shuttle *Challenger* disaster. Rubber O-rings composed of fluoroelastomers were used as seals between two sections of the solid-fuel rocket boosters. The elastic property required for proper function of the O-ring was only present at temperatures above the T_g. Engineers at the time rated this safe operating threshold to be 40 °F, while the temperature prior to launch was only about 28 °F (Rogers Commission, 1986). Shortly after launch, the O-rings failed to flex and perform the proper seals, causing pressurized hot gas from the solid rocket motor to reach and impinge on the external fuel tank, thus leading to explosion of the vessel. This tragic disaster prompted significant reform in the testing of polymeric materials, and continues to serve as an engineering case study.

The experimental measurement of T_g is performed accurately within a few degrees using one of several common laboratory methods. Differential scanning calorimetry (DSC), dynamic mechanical analysis (DMA), and thermomechanical analysis (TMA) are a few such techniques employed in industry. These techniques, although unique in experimental design and mechanism of action, all operate according to a similar template. Temperature is varied across a polymer sample, and an instantaneous spike in the value of a specific thermodynamic or physical property identifies the onset of the state transition, and thus determines the T_g.

The theoretical and computational prediction of the T_g, unlike experimental measurement, encompasses a multitude of approaches. Some models focus on the time-dependent structural relaxation mechanisms near the temperature of interest, while others instead rely on variables specific to the chemical structure of the polymer compound. Each model has its advantages and drawbacks, and often carries only selective applicability to certain classes of polymers. The proposal and refinement of such models, directed towards the goal of universal, fast, and reliable T_g prediction remain an area of strong research interest (Le et al., 2012).

The forthcoming sections of this report discuss some of the prevalent models used to characterize and predict T_g. First, amorphous materials and the glass transition are defined in a broad sense. The kinetics of the glass transition are then described using existing correlation functions that seek to define the response behavior and structural relaxation mechanisms of polymers. After an overview of the common laboratory techniques used to measure T_g, some existing empirical models used to predict T_g are introduced. The results obtained from these models are then assessed for accuracy and reliability by comparison with experimental values.

Chapter 1 – The Glass Transition

The glassy state has many practical implications in a multitude of industries, ranging from food processing to biochemical stabilization. The understanding of the glass transition is essential in achieving mastery of efficient production and processing of polymeric materials and other amorphous solids.

Structural glass is a subset of glassy materials that refer to conventional amorphous solid materials with configuration disorder. By definition, glass is non-crystalline, yet possesses some of the same mechanical properties as crystalline solids (Lubchenko & Wolynes, 2007). Glass is also viewed as a vitrified form of a supercooled, extremely viscous liquid that does not undergo viscous flow or structural rearrangement on any observable timescale (Angell & Goldstein, 1986). Preparation of these materials occurs by rapid cooling of a molten liquid, of which the cooling rate has a significant impact on the final product properties. The cooling rate must be sufficiently high to prevent crystallization, yet variably low to achieve the desired mechanical properties (Moynihan et al., 1974). It has been found that for different cooling rates, microstructural changes are nearly negligible while mechanical and relaxational properties may vary significantly (Painter & Coleman, 1997).

In measuring the value of a thermodynamic property P such as enthalpy against temperature T for a supercooled liquid undergoing a glass transition, various cooling rates yield different pathways. Thus, the temperature at which the given liquid experiences the transition is not static with respect to chemical structure and composition, but is instead dynamic and dependent on temporal effects.

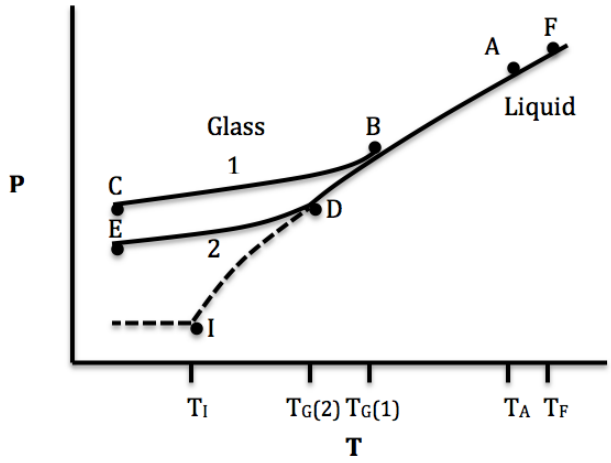

Figure 1: Variation of a thermodynamic property P vs. temperature T for a typical supercooled liquid in the glass transition region (adapted from Fredrickson, 1988)

In the above Figure 1, the liquid begins at state F and is supercooled to lower points on the curve. For a given cooling rate 1, the sample begins to transition to the glassy state at point B, completing the transition at point C along the diverted path as shown. However, choosing a slower cooling rate 2, the sample is able to remain in thermodynamic metastable equilibrium along the liquidus curve for longer, resulting in a lower glass transition temperature at point D. Both points B and D are nonequilibrium events termed laboratory glass transitions (LGT) (Gupta & Muaro, 2007). The theoretical minimum point at which the transition can occur by means of applying a minimum effective cooling rate is known as the ideal glass transition (IGT). The mechanism and ultimate existence of the IGT is often disputed in theory, with some researchers linking the IGT to either a thermodynamic or dynamical phase transition (Fredrickson, 1988). An underlying theme governing the latter transition type is that of ergodicity breaking, in which the time average behavior no longer coincides with the space averaged behavior (Palmer, 1982). This and other phenomena occurring near the glass transition temperature are subjects of active research in understanding the physical principles that govern the anomalous kinetics of structural glasses.

Chapter 2 – Response Behavior

2.1 Linear Response Properties

The linear regime of the relaxation behavior of supercooled liquids occurs as result of relatively small perturbations from metastable equilibrium. Depending on how far away one is from the glass transition temperature LGT, the behavior mechanism of the relaxation can be quite different. At temperatures well above LGT, most materials exhibit simple single-exponential behavior illustrated by the Debye relation (Goldstein & Simha, 1976):

$$\varphi(t) = e^{-t/\tau} \tag{1}$$

where $\varphi(t)$ is the linear response function and τ represents a characteristic structural relaxation time, which at this condition is governed by an Arrhenius relation (Roland, 2008):

$$\tau = \tau_0 e^{E/k_B T} \tag{2}$$

where *E* represents activation energy and k_B is the Boltzmann constant. However, as the temperature is lowered near the LGT, the observed time-dependent structural relaxation becomes a nonexponential relation. An effective model for describing this modified behavior is known as the stretched exponential and is given by the Kohlrausch-Williams-Watts (KWW) function (Williams & Watts, 1970):

$$\varphi(t) = e^{-(t/\tau)^{\beta}} \tag{3}$$

where β is simply $1/k_B T$ and is assumed to be less than 1.

A more fundamental view of Equation (3) can be expressed as (Debenedetti & Stillinger, 2001):

$$\varphi(t) = \frac{\sigma(t) - \sigma(\infty)}{\sigma(0) - \sigma(\infty)} \tag{4}$$

where σ is the measured physical quantity. This stretched exponential function marks the existence of distinct spatially heterogeneous relaxing domains developing from the slowing down of long-time relaxation (Ediger, 2000). However, the analysis of these domains is limited since it is unclear whether they relax exponentially or nonexponentially.

Subdivisions of supercooled liquids are created from the characteristic temperature dependence and magnitude of parameters τ and β. Liquids with a high temperature independent activation energy and low temperature dependent β value typically follow Equation (2) and are called strong liquids (Angell et al., 1986). Conversely, liquids with low activation energy and exhibiting non-Arrhenius behavior at low temperatures are termed fragile liquids (Angell et al., 1986). Some liquids exhibit properties of both strong and fragile liquids, and are deemed intermediate liquids (Böhmer et al., 1993). The temperature dependence of structural relaxation for these and fragile liquids can be expressed by the Vogel-Tamman-Fulcher (VTF) equation (Fulcher, 1925):

$$\tau = \tau_0 e^{E_0/(T-T_0)} \tag{5}$$

where τ_0, E_0, and T_0 are material-specific parameters independent of temperature. By virtue of the asymptotic relationship of the effective activation energy *E(T)* and temperature T_0, this relation assumes the existence of an IGT at T_0. As this assumption may not hold true for some liquids, the VTF equation should be selectively applied (Fredrickson, 1988).

An alternate expression for this temperature dependence of structural relaxation times is given by the Adam-Gibbs (AG) equation (Adam & Gibbs, 1965):

$$\tau = \tau_1 e^{E_1/TS_c} \quad (6)$$

where S_c is configurational entropy and is a function of temperature.

In this model, the origin of viscous slow-down close to LGT lies in the decrease in the number of configurations in the system, and structural arrest is predicted to occur at a specific temperature. However, the concept of a cooperatively rearranging region (CRR) was used in the derivation of this expression (Adam & Gibbs, 1965). The temperature variation across the CRR determines the temperature dependence on relaxation behavior (Ngai et al., 1991). The weakness in this approach is the lack of definition of the size as well as the indistinguishable nature of this region, since stretched exponential behavior is believed to be governed by heterogeneity. Nevertheless, Equation (6) describes relaxational behavior for deeply supercooled liquids effectively (Angell & Smith, 1982).

Equation (6) is also related to a theoretical inconsistency known as the Kauzmann Paradox (Kauzmann, 1948). Specifically, extrapolations of S_c to temperatures below LGT predict that S_c disappears at some temperature T_K, which happens to be the predicted structural arrest temperature in the AG theory (Kauzmann, 1948). At temperatures below T_K, configurational entropy is considered negative, which would violate the third law of thermodynamics unless some phase transition were to occur. Therefore, the validity of Equation (6) also depends on the existence of an IGT. Equation (5) is obtained from Equation (6) if the difference in heat capacities between the supercooled liquid and its stable crystalline form are assumed to be inversely proportional to temperature (Goldstein & Simha, 1976). Thus, Equation (6) should be at least as applicable as Equation (5), with the likelihood that it can be applied effectively to a greater variety of materials.

2.2 Nonlinear Response Properties

For large perturbations from metastable equilibrium, nonlinear time-dependent relaxation behavior is observed. In the nonlinear regime, the magnitude and sign of the perturbation affect the relaxation behavior. Temperature jump experiments reveal that relaxation from high and low temperature is asymmetric (Brawer, 1985). Specifically, for equivalent final temperatures and temperature jump values, an increase from a lower temperature will have a higher relaxation time than a decrease from a higher temperature (Fredrickson, 1988).

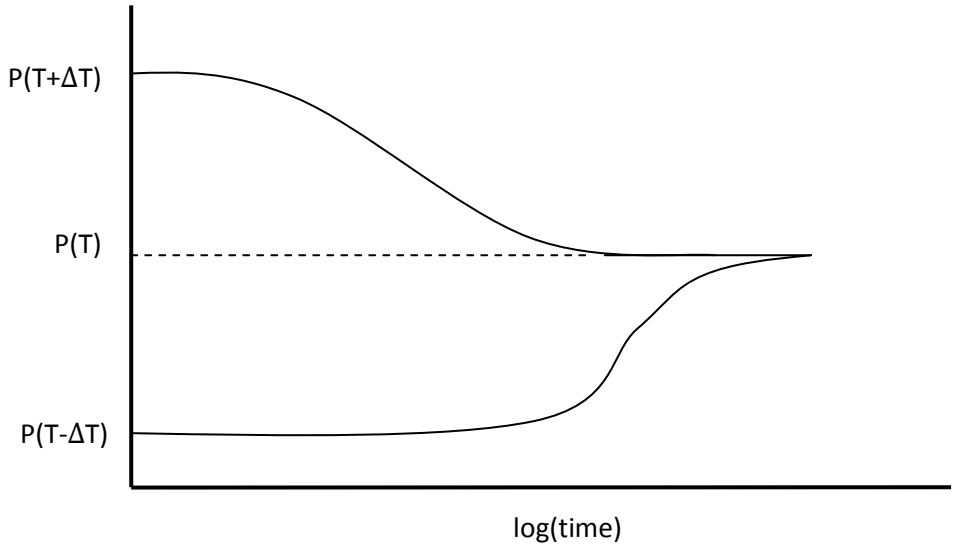

Figure 2: Temperature jump experiments in a supercooled liquid revealing asymmetric nonlinear structural relaxation (adapted from Fredrickson, 1988)

As seen in Figure 2 above, the final value of the temperature and thermodynamic property is the same in both experiments. In the experiment that begins at the lower temperature T-ΔT, the time to reach the equilibrium P value after the +ΔT jump to T is considerably larger. The qualitative behavior seen in Figure 2 will be observed when ΔT is sufficiently large.

Further insight into the nonlinear regime of structural relaxation can be seen in experiments that involve multiple temperature jumps of varying sign, commonly known as “crossover” experiments (Fredrickson, 1988). In one variation of a “crossover” experiment, an initial temperature above the LGT is subject to a negative jump to a point below the LGT, but then quickly followed by a positive increase at about half the initial jump magnitude. The result is an unexpected overshoot in the equilibrium property value at the final temperature (Brawer, 1985). This overshoot is often explained by entropy changes. The sign of vibrational entropy contributions is a function of the quenching direction (Scherer, 1992). Specifically, this contribution decreases after down quenching due to the drop in temperature. In this case, the sign of the translational and vibrational contributions are opposite, which gives rise to an entropy maximum. The crossover effect is observed at some T_x slightly greater than LGT, but only for appropriate magnitudes and kinetics of the various contributions (Brawer, 1985).

An alternate view reveals decoupling between translational diffusion and viscosity (Ediger, 2000) at a crossover point of $\mathrm{LGT} < T_x < 1.2 \cdot \mathrm{LGT}$. At this temperature, the inverse relationship between the translational diffusion coefficient and viscosity breaks down, although that for the rotational coefficient does not. A recent molecular dynamics (MD) simulation claims that the crossover effect can only be reproduced in simulations at sufficiently deep quenching temperatures and long aging times (Gupta & Muaro, 2007). Therefore, the study of crossover theory through MD is limited to these available conditions.

Chapter 3 - Molecular Dynamics

Simulations known as molecular dynamics (MD) obtain useful physical information about a system by carrying out an integration of the equations of motion over hundreds of particles. Standard conventions adopted to investigate supercooled liquids are a single-component system, equivalency of compression and cooling, and defined scales for variables such as time and length (Barrat & Klein, 1991). The most commonly obtained dynamical quantity in MD, the self-diffusion coefficient *D*, can be calculated using either the Einstein (7a) or Kubo (7b) formulas (Wang & Hou, 2012):

$$D = \lim_{t\to\infty} \frac{1}{6t} \langle [\boldsymbol{r}(t) - \boldsymbol{r}(0)]^2 \rangle \qquad (7a)$$

$$D = \frac{1}{3} \int_0^\infty \langle \boldsymbol{v}(t) \cdot \boldsymbol{v}(0) \rangle \, dt \qquad (7b)$$

where ***r*** and ***v*** represent position and velocity vectors, respectively. In supercooled liquids, *D* is typically small, primarily due to competing short-time and long-time mechanisms (Brawer, 1985). Thus, for supercooled liquids, the difference term in the mean squared displacement function offered in Equation (7a) is favorable over the velocity product of Equation (7b).

An extension of this expression leads to a parameter that can be interpreted as an order parameter for dynamic transition. Arising from the jump diffusion model, the Gaussian parameter can be written as (Barrat & Klein, 1991):

$$\alpha(t) = \frac{3}{5} \frac{\langle [\boldsymbol{r}(t) - \boldsymbol{r}(0)]^2 \rangle^2}{\langle [\boldsymbol{r}(t) - \boldsymbol{r}(0)]^4 \rangle} \qquad (8)$$

Deviations of $\alpha(t)$ from 1 indicate deviations from normal liquid behavior, and a stable non-unity value achieved at some time would indicate the presence of a new dynamic phase in the supercooled liquid (Bernu et. al, 1987). Obvious disadvantages to this MD method include the potential large timescale requirement, which may offset the convenience of the simple algorithm of the parameter.

Another analysis capability of interest in MD involves a spatial Fourier transform of the previously defined stretched exponential given by Equation (3). An expression known as the van Hove correlation function can be used to compute probabilities of finding particles at specific locations and times (Hopkins et. al, 2010). This expression can further be correlated with macroscopic hydrodynamics:

$$G_s(r,t) = N^{-1}\sum_{i=1}^{N}\langle\delta[\boldsymbol{r}_i(t) - \boldsymbol{r}_i(0) - \boldsymbol{r}]\rangle = \frac{1}{(4\pi Dt)^{3/2}}e^{-\left(\frac{r^2}{4Dt}\right)} \qquad (9)$$

The advantage of the latter expression in Equation (9) is that it gives rise to an opportunity to recognize structural arrest. Specifically, a plot of $4\pi r^2 G_s(r,t)$ vs. r/σ drastically changes shape at some critical crossover density n_x (Barrat et al., 1990). For $n > n_x$, diffusion seems to occur by neighbor jumps while for $n < n_x$ the diffusion behavior follows long-time hydrodynamics (Barrat & Klein, 1991). This approach proves useful in that the existence of a crossover point is clearly identifiable and can be fairly well fit to two distinct and comprehensible mechanisms. However, the precise quantitative point at which the transition occurs is difficult to identify with this method, as the precise time at which onset of a new curve shape occurs is subjective.

Other phenomena observed at the aforementioned crossover point prove useful in understanding the underlying physical mechanisms. While the transition is relatively broad, it can be more specifically marked by a change in the slope of the equation of state (EOS) (Bernu et al., 1987). Here, as the fluid undergoes structural arrest, a nonzero shear modulus also appears. The challenge in this approach is selecting the most appropriate EOS for the liquid. Once this challenge is met, this method is effective in providing more precise identification of the crossover point.

The appropriateness of approaches given by MD simulation may be system-specific, but the overall advantages and disadvantages of MD are summarized in Table 1:

Table 1: Advantages and disadvantages of MD simulation as applied to supercooled liquids

Advantages	Disadvantages
- Short run-time - Readily perform detailed calculations on simple particle interaction systems - Given access to multiple correlation functions - Simultaneously provide information on both structural and thermodynamic properties of a system	- Results quickly invalidated during ergodicity breaking phenomena - Limited workable timescale - Complications of component phase space for relaxation timescales greater than observed timescale - Properties may become a function of thermal history and current external thermodynamic parameters

Chapter 4 – Structural Relaxation Models

4.1 Kinetic and Hydrodynamic Models

The extension of hydrodynamics and kinetics to supercooled liquids offers considerable insight into the structural arrest mechanism. By applying nonlinear theory and mode-coupling, Leutheusser proposed a time correlation function in the form of a nonlinear integro-differential equation (Leutheusser, 1984):

$$\ddot{C}(t) + \gamma \dot{C}(t) + \Omega^2 C(t) + \Omega^2 \int_0^t M(t - t')\, C(t') dt' = 0 \qquad (10)$$

Here, *C(t)* represents a time correlation function and *M(t)* represents a memory function, with γ and Ω being damping and oscillation constants, respectively. By applying a low-order mode-coupling approximation to the memory function, Leutheusser was able to explicitly relate *C(t)* and *M(t)*, thus making the differential equation solvable for *C(t)* (Boone & Yip, 1991). The drawback to this approach, however, lies in the fact that it cannot be justified for timescales beyond the realm of high frequency expansions. Despite questionable validity, the Leutheusser model suggests that relaxation time follows a power law singularity and confirms the presence of the IGT (Fredrickson, 1988). This suggestion seems to follow experimental nonexponential behavior of some liquids (Taborek et al., 1986), and thus may possess some validity. The approach, however, is hindered because it neglects wave vectors related to density fluctuation. Since density fluctuations via a nonlinear feedback mechanism is the proposed driver of structural arrest in the model (Leutheusser, 1984), improved treatment of these vectors is essential for due diligence.

A better treatment of wave vectors using a similar approach to Leutheusser was performed by Bengtzelius and Kirkpatrick (1984), but arrived at many of the same results with only slightly modified exponents and relaxation spectrum broadness. These methods are also limited by the viscosity of the fluid, with fluids of viscosity beyond a certain threshold conflicting with molecular simulation results (Götze, & Sjögren, 1987) primarily due to the questionable mode-coupling theories that are used to relate *M(t)* to *C(t)*.

A model proposed by Das et al. (1985) employs basic fluid mechanics equations in the framework of hydrodynamic theory. The hydrodynamic model possesses a pressure term, convective term, dissipative term, and Gaussian noise term with no structural order parameters. Upon selection of an appropriate potential energy function, the results of this approach share many similarities with Leutheusser, including the feedback mechanism. However, it also introduces other nonlinearities, which cause the IGT to vanish while still retaining many of its effects (Das et al., 1985).

A summary of hydrodynamic relative to kinetic models appears in Table 2:

Table 2: A comparison of hydrodynamic and kinetic models for relaxation behavior of supercooled liquids

Advantages	Common Drawbacks	Disadvantages
- Not restricted to fluid type - Simple and precise - Extendable to higher order fluids	- Unknown correlation to structural order parameters - Questionable mode-coupling approximations	- Some parameters are found through questionable independent liquid theory equations - Uncertainty of wave vector dependence

4.2 Spin Models

Another approach in studying these liquid phase transitions is that of *n*-spin facilitated Ising models (nSFM) (Fredrickson & Andersen, 1984). In these models, spin-up is interpreted as a region of supercooled liquid with larger compressibility. With the imposition of a positive magnetic field, the number of these up-spins decreases with temperature. The flipping probability function is defined with high dependence on neighboring particles, thus leading to the theory of flipping by cooperative events, which becomes the proposed mechanism for relaxation (Fredrickson, 1988). One weakness of this approach is in the possibility of reducible dynamic constraints. In such a case, partitions would be necessary, which would lead to nonergodic behavior and thus alter the relaxation mechanism significantly. Therefore, the method essentially must depend on the appropriate restrictions.

The nSFM model can be reduced to specific choices of *n*. For example, the 1SFM model is used to represent isolated up-spins among a large number of down-spins. The immediate neighbor of the up-spin is allowed to flip-up while the original particle flips down, thus modeling a type of defect propagation analogous to a low-temperature relaxation mechanism (Fredrickson & Andersen, 1984). Monte Carlo (MC) simulations have confirmed that the 1SFM relaxation model obeys the Arrhenius expression of Equation (2) (Fredrickson, 1988). Overall, this model carries the advantage of being thermodynamically well-defined, but also relies heavily on a questionable spin-up conserving diffusion mechanism.

In the 2SFM view, surfaces of up-spins move in concert to relax surrounding down-spins through cooperative dynamics. Although perturbation theory predicted the existence of an IGT under this model, MC simulations have refuted this (Fredrickson, 1988). The simulations did, however, indicate nonexponential time decay and non-Arrhenius temperature dependence on relaxation (Angell & Goldstein, 1986). The results also indicate that 2SFM agrees well with the

AG Equation (6), but cannot be extrapolated to lower temperatures due to entropy function curvature (Dorfmüller & Williams, 1987).

Through application of various lattices and spin models, KWW (3) and VTF (5) behavior can also be derived (Fredrickson, 1988). Thus, the nSFM model is excellent as a supplement to other relaxation models, but as a standalone model may be too variable with respect to dynamic parameters to distinctively explain the glass transition.

4.3 Square Tiling Model

In a model proposed by Weber, Fredrickson, and Stillinger (1986), a supercooled liquid is represented by an area of squares of varying sizes. In this Square Tiling Model (STM), each square represents a region of liquid containing well-packed molecules while each boundary represents regions of weakened bonds between these liquid sections. It is predicted that at the phase transition, these interior walls become unstable and expand, which reduces the system to a single square domain of dimensions $L \times L$ (Weber et al., 1986). This model is dependent on the selection of an appropriate potential energy function, and is also limited by two-dimensional dynamics. An advantage to this is that the system is well contained, with area conservation being a strict constraint. However, any possible three-dimensional dynamic behavior is lost in such a model since all changes in the state of the system must be represented with two-dimensional phenomena. A visual representation of a square tiling model can be seen in Figure 3 below.

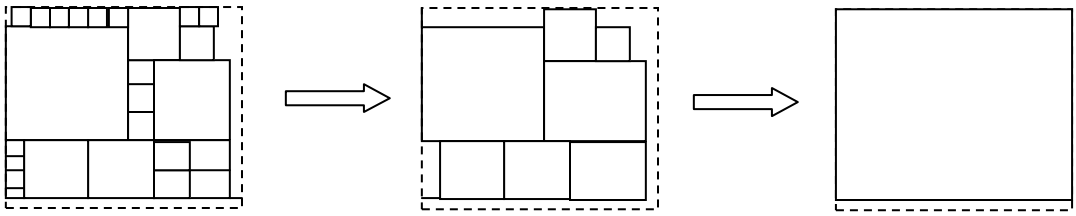

Figure 3: A sample evolution in a square tiling model representing structural relaxation

As seen in Figure 3, the boundaries of smaller squares collapse during relaxation to form larger squares. Relaxation is complete when only a single large square remains with a side length equal to the dimension of the defined system.

Two sub-models exist in this view (Weber et al., 1986), and are compared in Table 3:

Table 3: A comparison of square tiling sub-models using different kinetic rules

Model	Description	MC results	Disadvantages
Minimal aggregation	Square domains can fragment only if a dimensional condition is satisfied. Inverse aggregation is permitted.	- Relaxation occurs by KWW (3) behavior - Arrhenius (2) and AG (6) are not satisfied - Nonlinear phenomena	- Unconventional IGT with nonsingular relaxation times - Arbitrary long-range constraints
Boundary shift	Square domain can fragment into domains of unit squares. Inverse shift is permitted.	- KWW (3) behavior - Arrhenius (2) and AG (6) are not satisfied - Faster relaxation than minimal aggregation	- Dependent on identical domain sizes - Lattice spacing constraints

Chapter 5 – Experimental Measurement Techniques

Several laboratory techniques are available for the precise measurement of the glass transition temperature. The optimal technique is most often dependent on the physical properties and available sample volume of the compound to be measured.

5.1 Differential Scanning Calorimetry

A common thermoanalytical technique that can be applied to the identification and measurement of phase or state transitions such as the LGT is differential scanning calorimetry (DSC). In this technique, the temperature of experimental and reference samples is linearly increased and the corresponding amount of heat required is continuously measured. As the experimental sample undergoes a phase transition, more or less heat is required to maintain it at the same temperature as the reference, causing a spike to be observed on the recorded DSC signal. Specifically, in the case of the LGT, the sample undergoes a change in heat capacity even though no formal phase change occurs, and so the measured heat flow will experience a step increase at that temperature. Since this step generally occurs over the range of a few degrees, the LGT is taken to be the center point of the incline (Skoog, 1998).

Besides the state transition of the LGT, common phase transition temperatures measured via DSC include that of crystallization (T_c) and melting (T_m). Since crystallization is an exothermic process while melting is endothermic, the DSC signal experiences a negative and positive step, respectively, at these events. A typical DSC plot containing these transition points is shown in Figure 4. Values of T_m in relation to T_g for several common polymers are given in Appendix A.

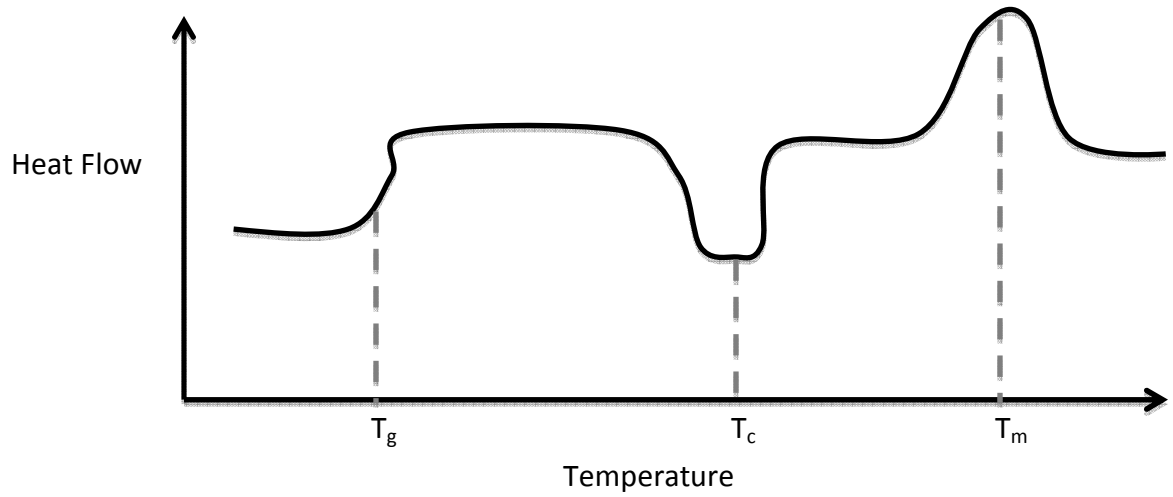

Figure 4: A typical differential scanning calorimetry plot with commonly identified state and phase transitions

5.2 Dynamic Mechanical Analysis

A very common method used in the characterization of the viscoelastic behavior of polymers is that of dynamic mechanical analysis (DMA). In this technique, a sinusoidal stress is applied to the test specimen and the magnitude and phase shift of the resulting strain is measured. Alternatively, the converse procedure may be employed in which strain is the input and the resulting stress is the measured output. With the gathered stress-strain data, one can compute the storage (E') and loss (E'') moduli as follows (Meyers & Chawla, 2010):

$$E' = \frac{\sigma_0}{\varepsilon_0}\cos(\delta) \tag{11}$$

$$E'' = \frac{\sigma_0}{\varepsilon_0}\sin(\delta) \tag{12}$$

where σ_0 is the stress magnitude, ε_0 is the strain magnitude, and δ is the phase lag between stress and strain.

In order to discern the LGT, the sample temperature is varied and compared against the resulting moduli in what is known as temperature-sweeping DMA. At the LGT, a dramatic decrease in the storage modulus along with a maximum in the loss modulus is observed. As seen through the combination of equations (11) and (12), this also equates to a peak in the ratio of *E''* to *E'* or $\tan(\delta)$, known as the material loss factor or loss tangent.

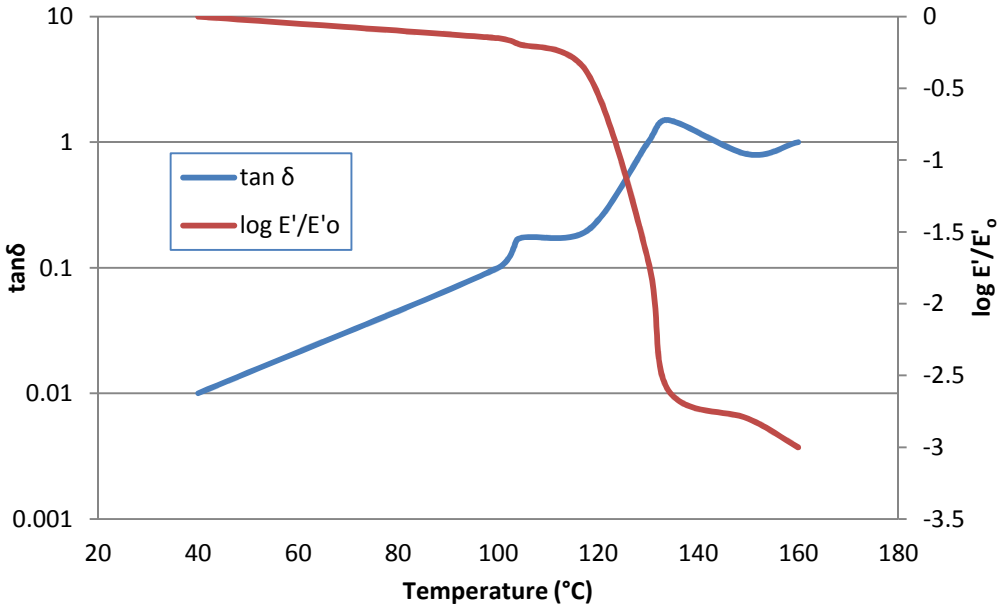

Figure 5: Temperature-sweep dynamic mechanical analysis spectra of the material loss factor and storage modulus for a PC/ABS polymer blend (adapted from Más et al., 2001)

While the LGT can be deduced from DMA data by either the peak *E''* or peak $\tan(\delta)$ value, the latter is the more prevalent in literature. The peak $\tan(\delta)$ value is several degrees higher than the peak *E''*, and corresponds more closely to the transition midpoint as opposed to the onset of the state transition (Seyler, 1994). As is evident from Equations (11) and (12), the peak in $\tan(\delta)$ arises from a compromise between the *E''* maximum and *E'* minimum. In Figure 5 above, the LGT is identified as being located roughly at 134 °C.

5.3 Thermomechanical Analysis and Dilatometry

Just as in DSC, another technique that utilizes a linear temperature program is thermomechanical analysis (TMA). With this method, a constant stress is applied to the polymer sample and the resulting dimensional changes are measured. Although the magnitude is held constant, the applied stress may be implemented in one of several directions and configurations including compression, tension, flexure, and torsion. So naturally, TMA lends itself to multiple instrumentation configuration geometries and a high degree of flexibility in experimental design. The heat transfer in a TMA is considerably slower than in a DSC, so the heating rates are typically limited to about 10 °C/min (Seyler, 1994).

The special case in which a flat-tipped probe is used to measure the expansion in a single dimension is referred to as linear thermodilatometry, and is a common method employed by many laboratories in determining the LGT (Earnest, 1994). Dilatometry is a technique qualitatively very similar to TMA in that the dimensional changes of a material are measured against temperature. Dilatometers, however, are generally used to measure expansion in larger samples. In the dimension of interest, samples measured in a dilatometer are typically 25 times longer than those measured by TMA. While dilatometers are generally more stable and easily calibrated, TMAs are especially suitable for thinner polymer samples on the order of less than 0.1 mm (Seyler, 1994).

The primary variable responsible for the dimensional change incurred by a polymer at the LGT is the coefficient of thermal expansion (CTE). The value of the CTE in the glassy state is low, but the increased degree of segmental molecular motion in the rubbery state causes the CTE to be relatively high. Therefore, the slope of the dimensional change versus temperature curve experiences a sizable increase at the LGT.

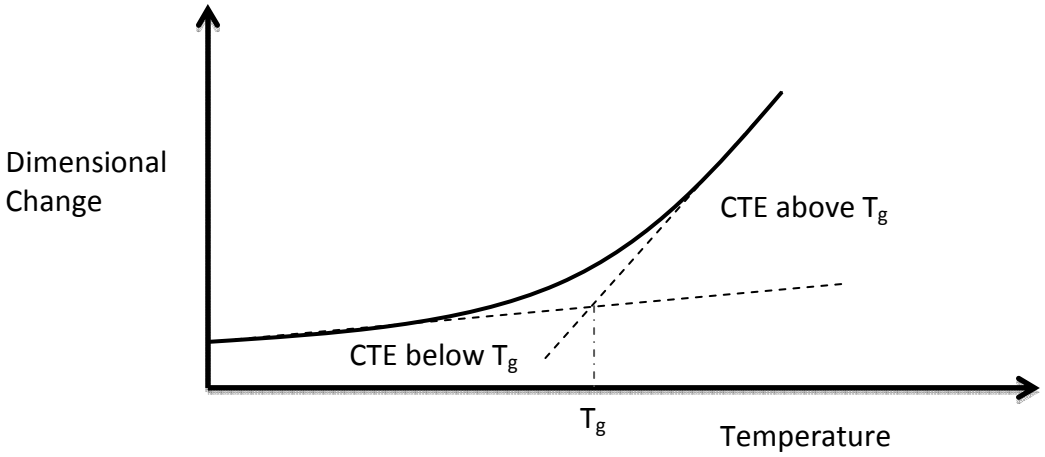

Figure 6: A typical thermomechanical analysis curve featuring the extrapolation of the glass transition temperature from the glass and rubbery CTE domains

While the transition as measured by the slope of the TMA curve may often be smooth, the LGT may still be measured accurately through the extrapolation of tangent lines. The intersection of these tangent lines representing the distinct linear domains serves as the approximation to the LGT, as illustrated in Figure 6 above.

5.4 Thermo-optical Analysis

A technique that relies more on visual observation is thermo-optical analysis (TOA). The polymer sample is subjected to a temperature program and the resulting light intensity is measured with a photocell. The physical property of birefringence, in which a material's refractive index is a function of light polarization and direction of propagation, encounters a drastic decrease at the LGT and thus serves as the basis of measurement. A significant advantage of this technique is in its ability to measure the LGT of very small samples, on the order of fractions of milligrams (Seyler, 1994). The primary disadvantage is in its inability to analyze transparent samples, which can be overcome by combining with DSC.

Table 4: **Comparison summary of common laboratory T_g measurement techniques**

Measurement Technique	Variable Exploited	Considerations
DSC	Heat Capacity	• Relatively large range of heating rates available • Larger samples should be run at lower heating rates • Smooth baseline with minimal noise required for accuracy
DMA	Energy complex moduli	• Good instrument temperature and force calibration required • Sample needs to have proper aspect ratio and even thickness • More sensitive than TMA
TMA	Coefficient of Thermal Expansion	• Advantage: Best for measuring thin (< 0.1 mm) samples • Dilatometer used for longer samples
TOA	Birefringence	• Advantage: Can measure very small samples • Disadvantage: Cannot analyze transparent samples • Can be combined with other techniques such as DSC

In addition to these general considerations, the optimal technique for a given sample can be determined empirically. By recognizing specific cases where peaks are indiscernible, an alternate setup or different technique should be elected. It is also worthy to note that since T_g occurs over a temperature range and these techniques are monitoring different processes, differences in measured T_g value of a few degrees are common and expected.

Chapter 6 – Polymer Glass Transition Temperature Predictor Models

As in supercooled liquids, the glass transition in polymers is similar to a second order phase transition. Thus, thermodynamic variables related to the second derivatives of the free energy will experience a discontinuity at the LGT (Van Dijk & Wakker, 1997). These include heat capacity, isothermal compressibility, and the CTE. Experimental techniques such as DMA, DSC, and TMA display this discontinuity in the form of a peak at the LGT. Such techniques are among the predominant methods for practical measurement of the LGT.

For design of new polymeric compounds and mixtures, however, it is useful to first predict the LGT prior to experimental measurement. Among other benefits, this allows for various potential product candidates to be surveyed prior to synthesis. As the desired application of the polymer often may involve temperatures very near to that of structural arrest and the LGT, fine resolution in accuracy is often required. Consequently, the development of simple and reliable LGT predictor models with wide applicability is of great value in industry.

Since polymer behavior is very much a function of thermal history, degradation effects from repeated application are a legitimate concern. When exposed to elevated temperatures near those that would constitute mechanical failure, polymers may undergo thermal degradation. In this process, the polymer is essentially fragmented into smaller molecules or monomers by one of several mechanisms including random scission, depolymerization, or side group elimination. However, although moderate changes in molecular weight commonly result, the LGT remains relatively insensitive to such changes (Crompton, 2010). As such, the consideration of only immediate thermal history along with base structural and thermodynamic features is generally sufficient to characterize properties near the LGT.

Studies of many polymer systems have shown that although properties of the glassy and transition regions are independent of chain length, the rubbery and liquid flow properties and their corresponding temperature range are markedly dependent on chain length (Bailey et. al, 1981). Besides chain length, various other structural properties of a given polymer play a key role in determining the temperature at which the glass transition will occur. While molecular weight is the central descriptor in many classic predictor models, variables that describe the chain stiffness and intermolecular forces in the polymer structure have also been found to profoundly impact the LGT. The appearance of specific constituent groups can also have a common influence, and often such variables prove to be more critical in certain classes of polymers over others.

6.1 Molecular Weight Relational Models

The earliest T_g models investigated the relationships that exist among a few of the most basic thermodynamic variables in a polymer. The polymer is first represented as a function of its constituent parts as $A(X)_pB$, in which *A* and *B* are the end groups, *X* is the repeating monomer unit, and *p* is the number of these monomer units or degree of polymerization. The molar volume *V* and molecular weight M can then be expressed as a sum of the contributions from the *p* monomer units and the end groups. Combining these two expressions through division leads to an equation for the specific volume for a polymer of degree of polymerization *p*:

$$v(p) = v(\infty) + \frac{V_e - m_e v(\infty)}{M} \tag{13}$$

where $v(\infty)$ is the limiting specific volume for a chain of infinite length, while V_e and m_e are the combined end chain molar volume and molecular weight, respectively.

Assuming a linear correlation between specific volume and temperature represented by coefficient α_p, Equation (13) can be rewritten as (Fox & Loshaek, 1955):

$$v(p) = v_0(\infty) + \alpha_\infty T + \frac{(m + m_e)(\Delta\alpha T + \Delta v_0)}{M} \quad (14)$$

where the subscript 0 represents a value extrapolated to a temperature of 0 K, m is the molecular weight of a single monomer unit, and a Δ represents the difference of a value at p = 1 and $p = \infty$. This expression completes a characterization of the interdependent behavior of volume, temperature, and molecular weight for a homologous series of polymeric liquids. The required parameters are obtainable from the structure and the $v - T$ curves for both the liquid monomer and infinite length polymer.

To relate v and T at the glass transition state, it is helpful to recognize that the transition occurs when the polymer encounters a drop in internal mobility that is related to the cooling rate time scale. It has been shown that this mobility value, sometimes referred to as segmental jumping frequency, is critically dependent on the specific volume and the following linear relationship holds (Bueche, 1953):

$$v_g = v_g(\infty) - B\left[T_g(\infty) - T_g\right] \quad (15)$$

where the subscript g represents the glass transition, B is a constant, and ∞ again indicates the limiting value for the infinite chain polymer.

Evaluating Equation (14) at the glass transition in both the generic and ∞ limit and substituting into Equation (15) leads to an equation that relates the glass transition temperature T_g to the molecular weight M for a given polymer:

$$T_g = T_g(\infty)\left[\frac{\alpha_\infty - B - \frac{(m+m_e)\Delta v_0}{T_g(\infty)M}}{\alpha_\infty - B + \frac{(m+m_e)\Delta\alpha}{M}}\right] \tag{16}$$

which can be rearranged and written as the Flory-Fox equation (Fox & Flory, 1950):

$$T_g = T_g(\infty) - \frac{K_g}{M} \tag{17}$$

where the empirical constant $K_g = (m+m_e)\left[\Delta\alpha T_g(\infty) + \Delta v_0\right]/(\alpha_\infty - B)$.

The constant K_g is related to the free volume in the sample, which is essentially a measure of the mobility of a polymer chain relative to its surrounding chains. As a polymer is cooled towards the LGT, free volume decreases until it eventually reaches a critical minimum value in which its chains are not free to move into alternate conformations. By virtue of its placement in a polymer chain, the end groups will account for a significantly higher fraction of the free volume available in a polymer chain compared to individual monomer units. For this reason, Equation (17) is accurately applied to high molecular weight compounds while only selectively applied to lower molecular weight polymers where the end groups would have a more profound influence.

There also exists a critical molecular weight for entanglement, above which T_g remains constant (Mark, 2004). Therefore, Equation (17) becomes theoretically invalid for molecular weights above this value in addition to being invalid below some lower bound. However, the molecular weight for entanglement is usually significantly large such that T_g calculated from Equation (17) is approximately $T_g(\infty)$, thus eliminating any upper bound of applicability. As a result, the Flory-Fox equation maintains accurate applicability for a wide molecular weight range. Just in the pilot study conducted by Fox and Flory (1950), empirical fitting of measured specific volumes for T_g determination in polystyrene was accurately performed in the molecular

weight range of 2,970 to 85,000 (Fox & Flory, 1950). The parameters of Equation (17) for polystyrene as determined in the pilot study were $T_g(\infty) = 373$ K and $K_g = 1.2 \times 10^{-5}$ (Fox & Loshaek, 1955). DSC measurements performed on polystyrene samples of varying molecular weight, however, showed the value of $T_g(\infty)$ to be approximately 381 K (Claudy et al., 1983). Applying this corrected parameter, Equation (17) for polystyrene is written as:

$$T_g = 381 - \frac{1.2 \times 10^{-5}}{M} \tag{18}$$

The calculated T_g values can then be compared to DSC measured values (Claudy et al., 1983) as shown in Table 5:

Table 5: Measured and calculated T_g values for polystyrene of various molecular weights using DSC and the Flory-Fox equation (Claudy et al., 1983)

M_w (g/mol)	T_g (K) measured	T_g (K) calculated
650	265.5	160
800	279	201
2100	328	321
2850	343	335
4000	353.1	349
17,500	369	374
37,000	378	377
275,000	379	380
600,000	380.5	381

The values in Table 5 suggest that Equation (17) carries reasonable accuracy of less than 2.4% error for polystyrene of molecular weight above approximately 2,100 g/mol. At low M_w values the end groups have a stronger influence and cause an overestimation of the sample free volume. In these cases, K_g is overestimated and the resulting predicted T_g value is lower.

A second polymer studied by Flory and Fox during the early formulation of Equation (17) was polyisobutylene. The parameter values as determined by Fox and Loshaek (1955) were $T_g(\infty) = 210$ K and $K_g = 0.3 \times 10^{-5}$. Comparing the calculated T_g values using Equation (17) and these parameters against recent reported measured values using DMA (Kunal et al., 2008) identifies a similar minimum bound of validity as shown in Table 6.

Table 6: Measured and calculated T_g values for polyisobutylene of various molecular weights using DMA and the Flory-Fox equation (Kunal et al., 2008)

M (g/mol)	T_g (K) measured	T_g (K) calculated
300	184.4	110
1100	191.1	183
2500	193.5	198
12,200	204.6	208

For polyisobutylene, an error of 4.2% is achieved at a number-averaged molecular weight of 1100 g/mol while a 2.3% error is present at 2500 g/mol. Thus, Equation (17) has been shown to be reasonably reliable for common polymers above a molecular weight threshold of approximately 2,000 g/mol.

From the original Flory-Fox equation came the rise of alternate molecular weight relational models, some of which are illustrated by the following equations (Fox & Loshaek, 1955, Dobkowski, 1982, and Ogawa, 1992):

$$\frac{1}{T_g} = \frac{1}{T_g(\infty)} + \frac{K_g}{T_g^2(\infty)M} \tag{19}$$

$$T_g = T_g(\infty) - \frac{K_b}{M + B} \tag{20}$$

$$\frac{1}{T_g} = \frac{1}{T_g(\infty)} + \frac{K_c}{M} \tag{21}$$

$$\ln T_g = \ln T_g(\infty) - \frac{K_d}{M} \tag{22}$$

$$T_g = T_g(\infty) - \frac{K_g}{\sqrt{M \cdot M_w}} \tag{23}$$

where K_b, K_c, and K_d are empirical constants and M_w is the weight-average molecular weight, used to supplement the standard number-average molecular weight M.

The overall accuracies of each of these equations are considered to be comparable (Kim et. al, 2008), and each shares many of the same essential characteristics. Specifically, each contains one or more empirical constants that must first be determined for the given polymer. In this way, the equations become usable only after a precedent is set for a given homologous series of a specific polymer. To do this, appropriate experimental data, generally in the form of dilatometric or viscometric measurements, must first be gathered and fitted to determine empirical parameters. Only then can the T_g of a varied molecular weight of an established polymeric compound be predicted. Therefore, for a polymer belonging to a newly discovered homologous series, the use of any of these equations offers no direct advantage relative to direct laboratory LGT measurement methods. Indirect advantages manifest when varied molecular weights within the given homologous series are being surveyed.

It is worthy to note that molecular weight relational models can also be applied to binary polymeric mixtures. Binary polymer mixtures are prevalent in industry, and are in fact often synthesized for the specific purpose of lowing the T_g. The secondary component in the mixture is commonly a diluent known as a plasticizer. This additive works to increase the free volume of the system and consequently lowers the T_g, thereby extending the rubbery regime to lower

temperatures. Since such mixtures are thermodynamically miscible, they are also miscible on a molecular scale. The blend exhibits a single LGT at a temperature intermediate to that of the respective constituent polymers. As the weight fraction of each polymer is altered, a systematic shift in the LGT also follows. The behavior of the LGT can be approximated as a composition averaged inversed additivity with respect to the constituents, written as the Fox equation as follows (Van Dijk & Wakker, 1997):

$$\frac{1}{T_g} = \frac{w_1}{T_{g,1}} + \frac{w_2}{T_{g,2}} \tag{24}$$

where w_1 and w_2 are the weight composition fraction of the respective constituent polymers. Equation (24) is most commonly applied in practice to polymer blends and statistical copolymers with great accuracy (Hiemenz & Lodge, 2007).

6.2 Disorientation Entropy Model

An alternate view of the glass transition uses the thermodynamic concept of configurational entropy as a central basis. Specifically, glass formation was suggested to arise from the loss of configurational entropy in the system, described as the vanishing number of configurational states accessible to the fluid at low temperatures (Gibbs & Di Marzio, 1958). The configurational entropy of a polymer system is relatively defined as:

$$S_c = S^{liquid} - S^{glass} \tag{25}$$

where S^{liquid} and S^{glass} indicate configurational entropies of liquid and glass states, respectively. In determining S_c for a given system, a reference zero state system is often used. This represents a “pure” or ideal polymer which lacks diluent molecules and possesses an ideal glass transition temperature, T_{g0}. Assuming the energy contribution from the vibration about

the lattice sites is negligible, S^{glass} = 0 in the reference zero system. Making the further assumption that the dependence of the number of polymer molecules n is equal on both the ideal and laboratory glass transition temperatures, S^{glass} = 0 in the real system as well.

However, unlike the reference zero system, the real polymer system possesses a heat capacity that is dependent on n. The corresponding expressions for S_c in the reference zero and real polymer systems can then be respectively written as (Chow, 1980):

$$S_c(0,T) = \int_{T_{g0}}^{T} \Delta C_p(T') d\ln T' \tag{26}$$

$$S_c(n,T) = \int_{T_g}^{T} \Delta C_p(n,T') d\ln T' \tag{27}$$

where ΔC_p is the difference in heat capacity between the supercooled liquid and glass.

Approximating transition increments of isobaric heat capacity as being independent of both temperature and composition, $\Delta C_p(n,T') = \Delta C_p(T') = \Delta C_p$. The real laboratory and ideal glass transition temperatures can then be related by the expression (Chow, 1980):

$$\ln\left(\frac{T_g}{T_{g0}}\right) = -\frac{1}{\Delta C_p}[S_c(n,T) - S_c(0,T)] \tag{28}$$

In proposing expressions for the configurational entropies, a model representation of the polymer liquid must first be chosen. In a given polymer solution exist solvent molecules and polymer molecules of varying size and chain configuration. These solutions preclude the standard conditions necessary for an entropy of mixing expression based on mole fractions of small molecules. In an alternative solution theory proposed by Flory and Huggins (1941), the polymer solution is represented as a collection of lattice sites that can be occupied by any of

the dissimilarly sized individual polymer segments or solvent molecules. Expressions for entropy can then be derived from statistical mechanics as functions of lattice volume fractions (Van Dijk & Wakker, 1997).

Employing the lattice model of Flory and Huggins, the S_c of a polymer can be considered to consist only of the polymer's disorientation entropy, such that $S_c(n,T) = S_{dis}$ and $S_c(0,T) = 0$. In this way, Equation (28) can be simplified to (Kim et. al, 2008):

$$\ln\frac{T_g}{T_{g0}} = -\frac{S_{dis}}{\Delta C_p} \tag{29}$$

where the disorientation entropy is expressed as a function of degree of polymerization (Lee et al., 2007):

$$S_{dis} = \frac{k_B \gamma_{dis}}{r}\left[\ln p + (p-1)\ln\left(\frac{z-1}{e}\right)\right] \tag{30}$$

where γ_{dis} is a proportional constant representing the degree of disorientation, and z is the lattice coordination number.

The combination of Equations (29) and (30) yields an expression that relates T_g to T_{g0}:

$$T_g = T_{g0}\exp\left[-\frac{\gamma_{dis}R}{\Delta C_p}\left(\frac{\ln p}{p} + \left(\frac{p-1}{p}\right)\ln\left(\frac{z-1}{e}\right)\right)\right] \tag{31}$$

where *R* is the ideal gas constant.

Since the ideal glass transition temperature T_{g0} is difficult to determine, T_g can instead be related to $T_g(\infty)$. The expression for $T_g(\infty)$ can be determined by taking Equation (31) to the $r \to \infty$ limit, which can then be divided from Equation (31) to obtain an expression for T_g as a function of p and constants associated with the given homologous series of polymers (Kim et al., 2008):

$$T_g = T_g(\infty)\exp\left[\frac{\gamma_{dis}R}{\Delta C_p p}\left(-\ln p + \ln\left(\frac{z-1}{e}\right)\right)\right] \quad (32)$$

Varying γ_{dis} while utilizing arbitrary sample parameter values of $T_g(\infty) = 400\ K$, $\Delta C_p = 20\ J/mol \cdot K$, and $z = 12$ illustrates the strong dependence of T_g on γ_{dis}:

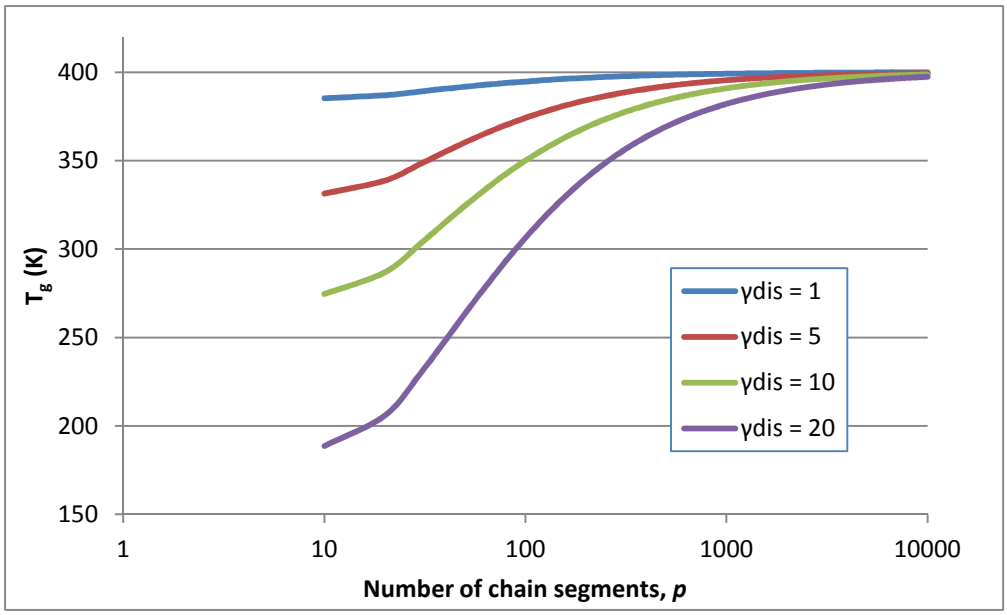

Figure 7: Theoretical prediction of T_g as a function of the number of chain segments for various degrees of disorientation using arbitrary constant sample parameter values (adapted from Kim et al., 2008)

As the number of chain segments increases, the relative volume of chain ends decreases and so a reduction in free volume of polymer occurs. In this way, T_g steadily increases with the number of chain segments. Eventually the value of T_g plateaus near a critical molecular weight of entanglement, which corresponds to some high number of chain segments. Also seen in Figure 7 is the larger range in T_g at higher values of γ_{dis}. Since a higher γ_{dis} value represents a greater disorientation of polymer chains, a corresponding increase in disorientation entropy also follows. In effect, the polymer chains experience greater flexibility and mobility across all values of p, and a consequently lower T_g.

For the application of Equation (32) toward the prediction of T_g for actual polymers, the value of γ_{dis} was found for a set of five distinct polymers by nonlinear regression, and appears along with corresponding ΔC_p and $T_g(\infty)$ values in Table 7 below (Kim et al., 2008):

Table 7: Disorientation entropy model parameters for various polymers (Kim et al., 2008)

Polymer	Abbreviation	ΔC_p $(J/mol \cdot \mathrm{K})$	$T_g(\infty)$ (K)	γ_{dis}	Monomer M_w (g/mol)
Poly(α-methyl styrene)	PMS	26.3	450	23.2	118.2
Poly(methyl methacrylate)	PMMA	32.7	385	9.7	100.1
Poly(vinyl chloride)	PVC	19.4	345	4.7	62.5
Polypropylene	PP	19.2	265	6.5	42.1
Poly(dimethyl siloxane)	PDMS	27.7	140	3.4	162.4

Using a lattice coordination number of z = 12 and comparing with DSC experimental data (Cowie, 1975), the continuous line curves plotted using Equation (32) are shown in Figure 8.

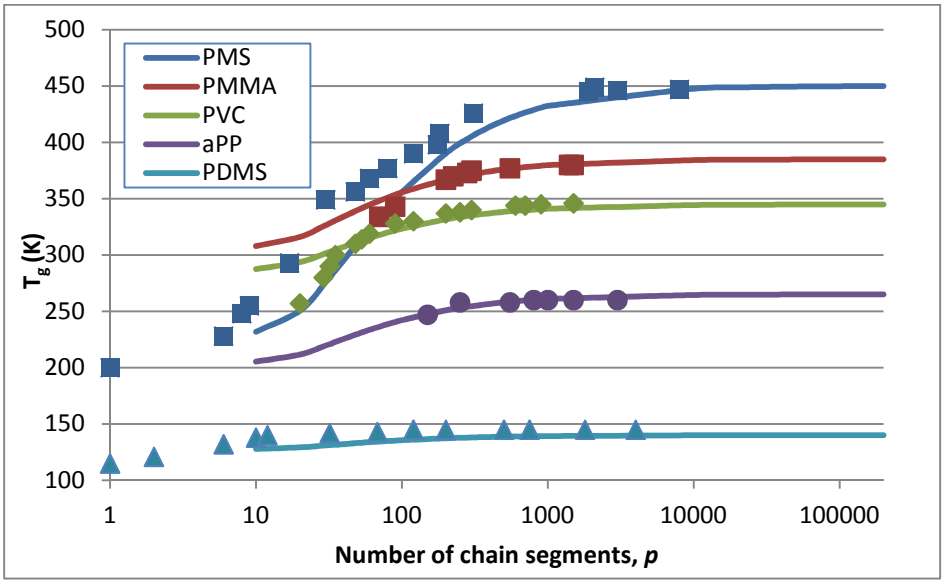

Figure 8: Comparison of T_g versus number of chain segments using disorientation entropy model (solid line) with reported DSC experimental values for various polymers (adapted from Kim et al., 2008)

As can be seen in Figure 8, the range of applicability of the disorientation entropy model for the theoretical prediction of T_g varies by polymer. For poly(dimethyl siloxane), the model seems to agree very well with experimental values all the way down to a molecular weight of about 1600 g/mol. On the other hand, the model T_g values for poly(α-methyl styrene) agree with experimental values well only down to about 20,000 g/mol. As expected, the polymers with smaller T_g range tend to have wider applicability with the disorientation entropy model. The data suggests that the model could be reliably used for polymer systems having $T_g(\infty) < 400\ K$ and greater than 100 chain segments.

6.3 Quantitative Structure-Property Relationship Models

Perhaps the most innovative approaches currently being taken in the prediction of glass transition temperature are those that focus on descriptors specific to the monomer. As the dependent variables are all related to the repeating unit structure, these models tend to be applied independently of polymer chain length (Katritzky et al., 1998). Thus, the polymers considered in such models are typically of large molecular weight past the critical value for entanglement. Essentially, these quantitative structure-property relationship (QSPR) models are estimating $T_g(\infty)$ for a given polymer, and can therefore be supplemented with molecular weight or configurational entropy models as an extension to other molecules in the given homologous series.

On the scale of a single polymer chain, the factors most affecting T_g are chain stiffness and intermolecular forces (Mark, 2004). Stiffness of polymer chains is most significantly affected by the barrier of rotation around carbon-carbon bonds in the backbone chain, which is most influenced by the size of the substituent group bonded to these carbon atoms. When the

backbone chain is allowed to rotate more freely, the T_g is effectively lowered. For example, for a polymer of generic structural formula $-(\mathrm{CH_2}-\mathrm{CHR})_n-$, a bulkier substituent group R yields a higher T_g while a longer side chain serves to lower the T_g (van Krevelen & Nijenhuis, 2009). Intermolecular forces are highlighted by the polarities of the repeating units and the hydrogen bonds that exist among the backbone chains and substituent groups. The T_g is effectively increased by stronger attractive forces between backbone chains and larger polarity or charge-induced dipole of the side group that works to limit the free motion of the molecule.

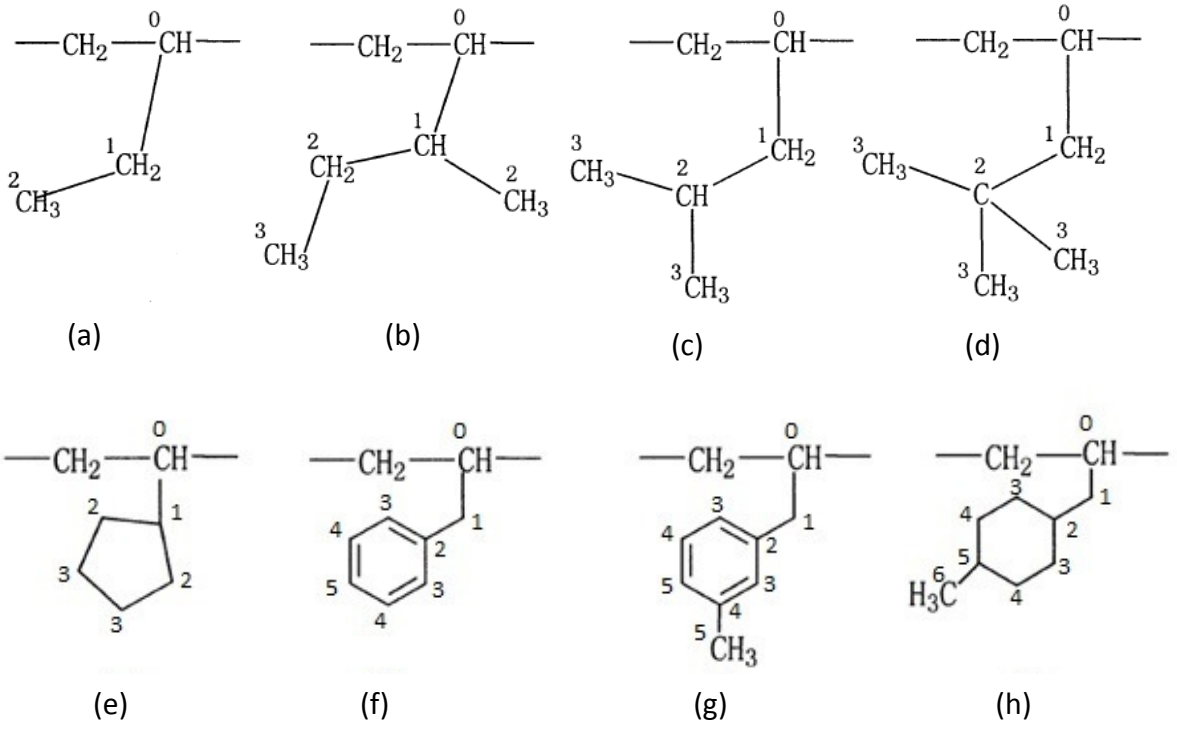

Figure 9: Repeating unit structures of polyethylenes with side chain C atoms labeled by bond distance from backbone chain (adapted from Cao & Lin, 2003)

It has been found that the size consideration that most affects the T_g in polyethylenes is not the total size of the substituent group R, but is instead the size of the terminal group in the substituent group R (Cao & Lin, 2003). Therefore, parameters chosen for the chain stiffness

variable of the model include the volume of the terminal group, MV_{ter}, in the substituent group R and the free length, L_F, of side chain (Cao & Lin, 2003).

As illustrated in Figure 9, the determination of lengths on the side chain is a straightforward task. The number above each carbon atom represents its minimum bond distance from the backbone chain carbon atom. To determine L_F, however, one must compute the length discrepancy between the side chain and its terminal group (van Krevelen & Nijenhuis, 2009). In polymer (a), the ${}^2C - {}^1C$ bond of the terminal group is able to rotate freely around the ${}^1C - {}^0C$ bond. Similarly, the terminal ${}^3C - {}^2C$ bond is free to rotate around the ${}^2C - {}^1C$ bond in polymer (b). Polymers (c) and (d), on the other hand, contain multiple equivalent terminal groups. In polymer (c), it is necessarily true that if one of the two ${}^3C - {}^2C$ bonds rotates around the ${}^2C - {}^1C$ bond, the other ${}^3C - {}^2C$ bond does as well. Similarly, all three ${}^3C - {}^2C$ bonds in polymer (d) rotate simultaneously around the ${}^2C - {}^1C$ bond. If effect, the non-free rotation terminal parts of the side chains for polymers (a)-(d) are $-CH_3, -CH_3, -CH(CH_3)_2, \text{and} -C(CH_3)_3$, respectively. The length discrepancy between the side chain and its corresponding terminal group can then be computed to determine the free length, L_F. Together with the cyclopentyl, phenyl, methyl-phenyl, and methyl-cyclohexyl terminal groups of polymers (e)-(h), the L_F values for polymers (a)-(h) become 1, 2, 1, 1, 0, 1, 1, and 1, respectively (Cao & Lin, 2003).

Terminal group volume, MV_{ter}, can be calculated using one of a variety of molecular software packages. For a polymer $-(\mathrm{CH_2} - \mathrm{CR^1R^2})_n -$ containing two side groups $\mathrm{R^1}$ and $\mathrm{R^2}$, it has been found that the resulting T_g is lower in the case where the two side groups are equal, $\mathrm{R^1} = \mathrm{R^2}$, than if they are different (Cao & Lin, 2003). Therefore, the influence of the substituent group R on T_g is dependent on molecular symmetry. The backbone chain of a symmetric substituted polymer seems to rotate more freely than for its asymmetrical counterpart. To capture the varied T_g influence in the two cases, a sum volume of terminal

groups can be used as the MV_{ter} parameter for the asymmetrical substituted polymer while a margin volume can be used for the symmetrical case. With a regression fit, the two parameters L_F and MV_{ter} are sufficient for relatively accurate prediction of T_g for nonpolar repeating units (Cao & Lin, 2003).

Monomer units that possess polarity require incorporation of parameters that capture the prevalent intermolecular forces. For a given polar repeating unit polymer, $-(\mathrm{CH_2}-\mathrm{CYZ})_n-$, the relative polarity of the monomer unit results from discrepancies in electronegativity between the Y and Z side groups as well as between the CH_2 and CYZ groups, along with polarizability effects of Y and Z (Bicerano, 2002). The presence of specific functional groups in Y and Z will also have marked effects on the main chains of the polymer. If an –OH or –NH group exists in the side groups, a hydrogen bond may be formed between polymer main chains. The existence of a $-\mathrm{C}\equiv\mathrm{N}$ group, on the other hand, would present an additional electrostatic attraction between main chains (Mark, 2004). Either of these added interactions would work to enhance the forces between the polymer backbone chains, thus limiting their ability to freely rotate. These intermolecular force effects can be effectively described by the introduction of three new parameters: the substituted backbone electronegativity discrepancy ΔX_{SB}, the polarizability effect $\sum \mathrm{PEI}$ of side group, and the electrostatic attraction $Q_{\pm}$due to hydrogen bond between the polymer main chains (Cao & Lin, 2003).

Electronegativity discrepancy ΔX_{SB} for the $\mathrm{CH_2}-\mathrm{CYZ}$ monomer unit can be calculated as the geometric mean of $|X_Y - X_Z|$ and $\left|X_{CH_2} - X_{CYZ}\right|$, expressed as (Katritzky et al., 1998):

$$\Delta X_{SB} = \sqrt{|X_Y - X_Z| \cdot \left|X_{CH_2} - X_{CYZ}\right|} \tag{33}$$

where any given group electronegativity $X_{eq}$is computed via an equalization method using Pauling electronegativity units (Bratsch, 1984):

$$X_{eq} = \frac{\sum_i \nu_i + q}{\sum_i \frac{\nu_i}{X_i}} \tag{34}$$

where ν_i is the number of i atoms, q is the overall integral charge of the group, and X_i is the initial pre-bonded electronegativity of atom i. The polarizability effect is computed as a sum over individual essential unit polarizability values and bond angles via the following expression (Chenzhong, C., and L. Zhiliang, 1998):

$$\sum PEI = \sum \left(\sum \frac{\alpha_i}{\left[N_i \frac{1+cos\theta}{1-cos\theta} - \frac{2cos\theta(1-cos^{N_i}\theta)}{(1-cos\theta)^2} \right]^2} \right) \tag{35}$$

where α_i is the polarizability of the ith essential unit in the substituent, N_i is the carbon atom number from the point charge q to the ith essential unit, and θ is the $\angle CCC$ bond angle supplement. Atomic values for α_i , much like atomic electronegativity values X_i , are readily available in literature (Haynes, 2011):

Table 8: Atomic polarizabilities and Pauling electronegativities of common atoms

Atom:	**H**	**C**	**N**	**O**	**F**	**Cl**	**Br**	**I**	**S**	**P**
α_i $(10^{-24}\ \mathrm{cm}^3)$	0.667	1.76	1.10	0.802	0.557	2.18	3.05	5.34	2.90	3.63
X_i	2.20	2.55	3.04	3.44	3.98	3.16	2.96	2.66	2.58	2.19

The final intermolecular force parameter, the electrostatic attraction $Q_{\pm}$ due to hydrogen bond, is computed in cases where a hydrogen bond exists between the main chains, such as when a side group contains an –OH or -NH. The value of $Q_{\pm}$is computed as a product of part charges on the two atoms again using Pauling units and the equalization method. For the generic bond $-\mathrm{MH}$ in a side group, the expression becomes (Bratsch, 1984):

$$Q_{\pm} = q_M q_H \tag{36}$$

where partial charge q_i is equal to $v_i(X_{eq} - X_i)/X_i$. As seen in Appendix B, a majority of polymers do not have a hydrogen bond connecting main chains (Katritzky et al., 1998), and thus have $Q_{\pm} = 0$. For polymers that do contain the hydrogen bond between main chains, $Q_{\pm}$ possesses a negative value.

The five molecular descriptors that serve as parameters can be summarized by the variables $\sum MV_{ter}(R_{ter}), L_F, \Delta X_{SB}, \sum PEI$, $and\ Q_{\pm}$. Through interrelation analysis, it was found that these five parameters are all significant descriptors in the model and are independent of each other, and the correlation with T_g produces a first order regression equation (Cao & Lin, 2003):

$$T_g\ (K) = 203.97(\pm 5.58) + 0.39(\pm 0.03) \sum MV_{ter}(R_{ter}) - 8.93(\pm 0.90) L_F + 138.82(\pm 12.33) \Delta X_{SB} + 9.01(\pm 2.18) \sum PEI - 1174.41(\pm 216.89) Q_{\pm} \quad (37)$$

In developing this model, a training set of 22 linear polymers of medium molecular weight were used (Cao & Lin, 2003). After successful formulation of the regression equation constants, the T_g of other polymers can be predicted using Equation (37). Compared with experimental data for a set of 88 diverse polymers (Katritzky et al., 1998), the statistical R^2 value for the fit was 0.9056 with a standard deviation of 20.86 K and absolute average error of 15.30 K (Cao & Lin, 2003). This indicates a reasonably good correlation for the model with the prediction of T_g, but with significant issues in reliability for select polymers. For example, the predicted T_g for poly(3,3-dimethylbutyl methacrylate) was 377 K, while the experimental value was only 318 K, producing an error of 18.6%. A complete listing of data for all 88 polymers can be found in Appendix B. Unfortunately, no common distinctive feature among the poorly estimated polymers could be identified, and the scatter plot shown in Figure 10 below reveals a relatively uniform error distribution.

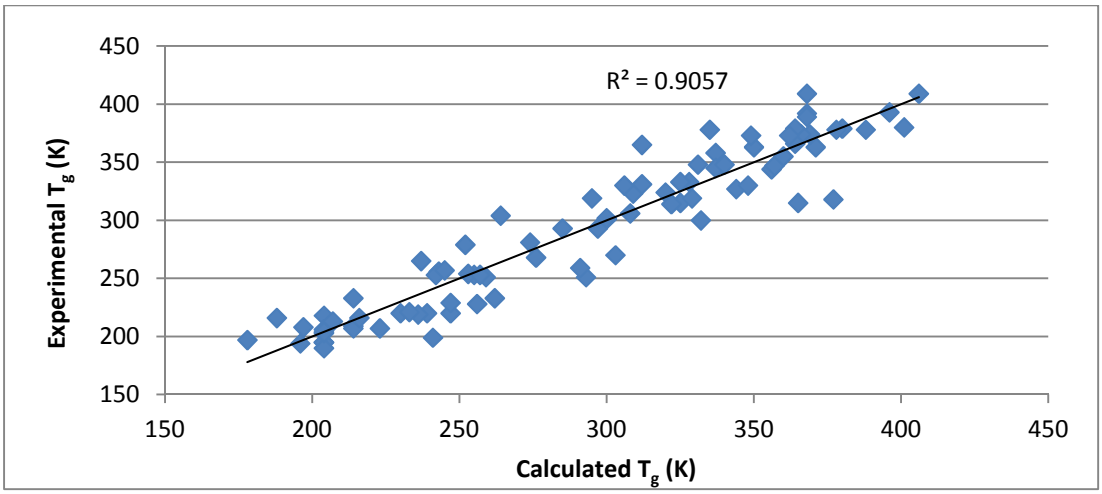

Figure 10: Experimental versus calculated T_g values using 5-descriptor QSPR model

By employing the same template of a model driven by monomer unit descriptor parameters, many similar QSPR models have been derived and applied with comparable results. Models derived in current research typically rely more heavily on molecular software packages to extract and calculate the relevant molecular descriptor variables. Through the use of novel computational techniques such as density functional theory (DFT), monomer structures can be optimized for analysis during modeling (Katritzky et al., 1998).

In a recent study, a total of 1,664 molecular descriptors were calculated for each of 105 polyacrylate and polyvinyl molecules using DFT (Yu, Yu, & Wang, 2009). Multiple linear regression (MLR) with a training set of 50 experimental T_g values was then used to seek an optimum subset of descriptors for incorporation into the model. For simplicity and robustness, only a few descriptors were sought for complete characterization of T_g. Ultimately, the optimal MLR model contained just three descriptor parameters, with physical meanings comparable to that of the 5-descriptor model previously discussed. Specifically, the descriptors used were mean atomic van der Waals volume, Mv, bond information content, $BIC5$, and electron diffraction 3D structure representation, $Mor13m$ (Yu, Yu, & Wang, 2009). Similar to the

parameters of the previous model, these variables work to describe the chain stiffness and molecular mobility of the polymer. A statistical fit produced a corresponding regression equation (Yu, Yu, & Wang, 2009):

$$T_g = 73.050 + 698.016Mv - 278.545BIC5 - 54.569Mor13m \quad (38)$$

The statistical R^2 value for the fit was only 0.861 with a standard deviation of 20.9 K, and the absolute error for the test set was approximately 21.7 K. Some improvement was achieved through the use of an alternate method to MLR known as an artificial neural network (ANN), in which the test set error was reduced to 17.7 K (Yu, Yu, & Wang, 2009). The overall results using this model were comparable to those seen in the previous model, with complete input parameter and output T_g values tabulated in Appendix C.

Table 9: Comparison of predicted T_g values obtained from 5-descriptor and 3-descriptor QSPR models for various polymers ([a]Cao & Lin, 2003 and [b]Yu, Yu, & Wang, 2009)

Polymer	$T_g\ (K)\ \ calc^a$ 5-descriptor	$T_g\ (K)\ \ calc^b$ 3-descriptor	$T_g\ (K)$ experimental
Poly(1-heptene)	230	224	220
Poly(3-methyl-1-butene)	309	395	323
Poly(3-pentyl acrylate)	245	271	257
Poly(3-phenyl-1-propene)	325	314	333
Poly(4-methyl-1-pentene)	300	303	302
Poly(acrylic acid)	380	401	379
Poly(ethyl acrylate)	259	232	251
Poly(methyl acrylate)	274	312	281
Poly(*sec*-butyl acrylate)	255	237	253
Poly(*tert*-butyl acrylate)	325	325	315
Poly(vinyl acetal)	360	359	355
Poly(vinyl acetate)	300	292	301
Poly(vinyl chloroacetate)	264	305	304
Poly(vinyl *n*-butyl ether)	233	226	221
Poly(vinyl *n*-octyl ether)	196	218	194
Poly(vinyl *n*-pentyl ether)	223	218	207
Poly(vinyl *sec*-butyl ether)	242	245	253
Poly(vinyl trifluoroacetate)	295	294	319

As shown in Table 9 and Figure 11, significant differences in the predicted T_g values exist between the two QSPR models. The T_g value for poly(3-methyl-1-butene) is predicted with significantly greater accuracy using the 5-descriptor model (4.3% error) versus the 3-descriptor model (22.3% error), but the T_g for poly(vinyl chloroacetate) is better predicted using the 5-descriptor model (0.3% versus 13.2% error). Since these models are constructed via regression and use different parameters, accuracy differences will exist for many polymers without easily identifiable molecular justification. The ratio of the test set to training set of polymers was 4:1 and 2.1:1 for the 5-descriptor and 3-descriptor models, respectively. Therefore, since more of the predictor set was used to develop the model regression equation, the 3-descriptor model equation has an advantage in relative accuracy. The disadvantage resulting from the fewer number of descriptors works to offset this advantage and make the two models rather competitive in accuracy.

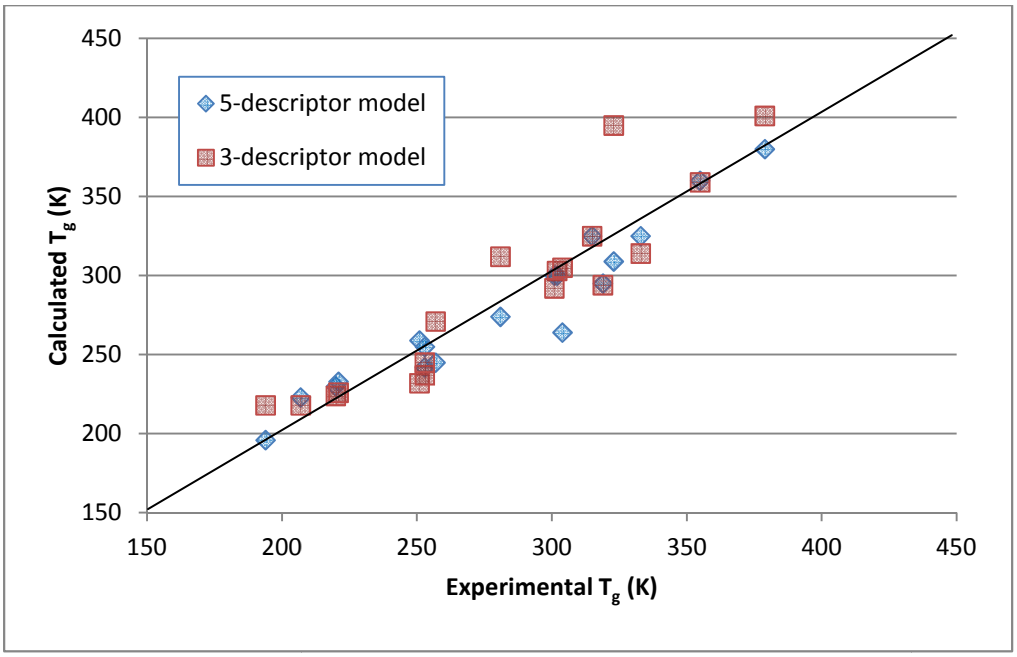

Figure 11: Calculated versus experimental T_g values for various common polymers using 3-descriptor and 5-descriptor QSPR models

As seen in Figure 11 above, the largest differences between the two QSPR models for the common polymers surveyed exist in the 280-305 K experimental T_g range. In this range, the 5-descriptor model tended to more greatly underestimate the T_g than did the 3-descriptor model. While some specific conclusions on the relative performance of the two models can be drawn for this specific set of polymers, it would be expected that a different set of polymers would yield significantly different results.

Chapter 7 – Discussion and Conclusions

The recent strides towards understanding the glass transition in supercooled liquids have been among the most significant in the history of the subject. The capabilities lent by molecular simulation have been proven to support proposed theories concerning the mechanism of the crossover point in these liquids, and continue to be invaluable in this area of research.

In the literature, the glass transition has been shown to be dependent on temporal effects. Studies have shown that for a polymeric liquid starting at some temperature in the rubbery regime, the cooling rate will impact the precise value of T_g. The minimum possible T_g, referred to as the ideal T_g or IGT, has often been disputed in theory. Ultimately, research has been inconclusive as to whether a precise and unique IGT exists for any given polymer, and if it does exist the associated mechanism is also uncertain.

The current state-of-the-art models on glass transition include various linear and nonlinear relaxation correlations, which include those presented as Debye, KWW, Arrhenius, VTF, and AG in Equations (1) through (6). These response theories have been coupled with various dynamic models in the literature to describe structural relaxation. Many of these models have been shown to possess adequate simplicity to be solved effectively by analytical or simulation methods. MD simulations have been used in several studies to obtain useful results. These studies have been able to identify the point at which structural arrest seems to occur, but only within a reportedly broad range.

In other studies, kinetic and hydrodynamic models have been constructed through the application of theory involving principles such as mode-coupling, nonlinearity, wave vectors, and fluid mechanics. The Leutheusser and Bengtzelius & Kirkpatrick models both concluded

that the unique IGT exists and relaxation time follows a power law singularity, but the Das model differed by concluding that an IGT does not exist.

Another work presented nSFM models as a means of describing the structural relaxation mechanism. In this family of models, polymer particles encountered flipping from a spin-up to a spin-down state with increasingly higher probability as temperature decreased. Supporting studies used MC simulations to conclude that nSFM models indicate nonexponential time decay and non-Arrhenius temperature dependence on relaxation. These MC simulations also concluded that the IGT does not exist in this model, although a separate study using perturbation theory indicated that the IGT does exist under the nSFM model.

In another study, MC simulations were also applied to an STM model. This two-dimensional model represented a polymeric liquid as an area of squares whose individual boundaries become unstable and vanish at decreasing temperatures. The MC simulations reportedly confirmed the existence of the IGT and showed structural relaxation to follow nonexponential behavior as illustrated by the KWW relation in Equation (3).

The results of many of these models don't agree on some key aspects. In studying all of the mentioned models, one is still not certain of the presence of an IGT, as models such as the STM reveal an IGT while those such as 2SFM or hydrodynamic models proposed by Das refute the presence of an IGT yet reveal some of the same characteristics associated with the phenomenon. The validity of some of the models is also questionable. For example, the simplifying assumptions made in the Leutheusser and Bengtzelius & Kirkpatrick models used mode-coupling approximations that are not justifiable at all timescales. The nSFM model relies on a questionable spin-up conserving diffusion mechanism and the STM model ignores three-dimensional phenomena. With any model of a desired simplicity, however, these types of disputable simplifying assumptions are bound to exist. In the end, these models are still able to

provide considerable insight into the behavior of polymers near their T_g. The primary consensus that can be reached from all these theoretical models is the existence of a temperature-dependent structural relaxation mechanism, of which the physical particulars are likely fluid-specific and involving multiple phenomena.

Much further work is needed to advance the subject of the glass transition. Primarily, a better understanding of the temperature region between the crossover temperature and the glass transition temperature must be achieved through better characterization of atomic motion, testing of multiple mode-coupling theories quantitatively, and also the testing of spin and square-tiling models quantitatively. Also, from the hydrodynamic end, the testing of non-Newtonian equations of motion may be appropriate for short-time dynamics. Hydrodynamic models that also incorporate molecular structure could be introduced and analyzed by MD to identify structural order parameters.

The relation between multiple relaxation behavior models provides endless research opportunities. For example, a connection between the hydrodynamic and spin models could aid in a construction of a hybrid hydrodynamic model with long-wavelength, low-frequency dynamics. Proving that the AG relation (6) holds for all nSFM models can be achieved by simulations with n > 2. Also, expanding on kinetic rules in the Square-Tiling model may give rise to other fragmentation mechanisms that translate to alternate modes of relaxation. Perhaps even application of pressure can introduce shifts in the crossover point and thus be incorporated into some future models.

Apart from understanding the relaxation behavior of polymers, the ability to predict T_g quickly and reliably is of great interest. The primary basis of comparison is with the results obtained from experimental measurement. Novel empirical models that employ QSPR theory have been shown to have considerable accuracy and a great potential for improvement.

The experimental techniques described in the literature as being most utilized in industry all share a common template. The value of a physical or thermodynamic variable known to drastically change at the T_g is measured across temperatures that span the T_g, and the observed spike is recorded and identified with the T_g. While it has been shown that most polymers can be accurately analyzed by any of the techniques discussed, limiting factors such as sample size and transparency naturally favor some techniques over others. For example, TOA was described as being best capable of measuring T_g for very small samples but unable to analyze transparent samples. TMA was shown to be better suited to thinner samples while dilatometry was described as being applicable for larger samples. Since T_g occurs over a temperature range and different experimental techniques monitor different thermodynamic processes, measurement variability of a few degrees between different techniques is common.

Several T_g predictor models have been well described through previous studies. The early models were molecular weight relational and were derived using basic relationships between volume, molecular weight, and temperature. Equations (17) – (23) summarize this class of models, which all report to have fairly good accuracy. Another class of predictor models uses configurational entropy as a central basis. One example of such a model used parameters related to disorientation entropy to predict T_g. The published results showed that accuracy was generally very good for polymers possessing a large number of chain segments.

The T_g predictor models published most recently were generally of the QSPR type. The parameters in these models were illustrated to be a function of the monomer unit, and so the

models were said to be only applicable to polymers of large molecular weight. Using modern computation techniques, a large number of potential molecular descriptors were surveyed and effectively chosen via multiple linear regression or more advanced algorithms. The underlying phenomena of the relevant variables used in such models were related to chain stiffness and intermolecular forces within a given monomer unit. The accuracy of these advanced models have been reported to be on the order of about 20 K.

While the physical properties and characteristic temperatures of a polymer may vary significantly with varied applied cooling rates, practical considerations are typically performed at static operating temperatures. As the polymer possesses consistent behavior in isothermal and isobaric operation, a single T_g can be effectively evaluated. While multiple laboratory techniques are readily available to accomplish this measurement for a given polymer sample, models to predict T_g for new polymers are useful in surveying potential products for a given application. Selection of the appropriate model is first and foremost dependent on experimental precedent. Should varying chain lengths within a given established homologous series of polymer be considered, molecular weight relational models illustrated by Equations (17)-(23) or configurational entropy models such as that represented by Equation (32) are most appropriate. The necessary input variables to these model equations such as $T_g(\infty)$ and other polymer-specific constants must first be established through an experimental precedent. The reliability of these models is generally good to a lower bound of about 2,000 g/mol of molecular weight or a couple hundred chain lengths, and a maximum $T_g(\infty)$ of about 400 K.

For new polymers without an experimental precedent, quantitative structure-property relationship (QSPR) models that focus on structural characteristics of the monomer are most appropriate. Properties related to the terminal groups in these repeating units have proven to be key in predicting T_g, with bulkier terminal groups and lower free chain length raising T_g.

Larger intermolecular forces arising from polarity or strong hydrogen bonding between main chains have also been found to serve as a barrier to free rotation and thus also increase T_g. Overall, QSPR models have proven to correlate well with experimental T_g data, the better models achieving a statistical $R^2 > 0.90$ and average absolute errors of less than 20 K, or approximately 6%.

For T_g predictor models, given that the variability in experimental measurement is as high as 5-10 K, absolute errors of less than 20 K are relatively satisfactory. The focus must be on achieving this level of accuracy across all polymers, as some polymers have shown to be statistical outliers with regards to measured accuracy. The reliability of the model regression equations can likely be increased by using a larger training set of more diverse polymers. The number of potential forms of molecular weight relational model equations have nearly been exhausted, all showing good mean accuracy above a certain chain length number threshold. Greater opportunity for improvement exists in the refinement of configurational entropy models, as a wide array of factors that may affect entropy exist as potential variable candidates. Prediction of T_g for polymers of low molecular weight remains the biggest challenge.

While the average performance of the most novel QSPR models is satisfactory, refinement is necessary to also address certain polymer cases that yield larger errors. Perhaps an advanced multiple linear regression analysis of molecular characteristics of polymers yielding high T_g value errors could illuminate additional relevant variables. Sacrificing simplicity may be appropriate, as extending models to incorporate additional molecular descriptor variables may yield improved accuracy.

References

Adam, Gerold, and Julian H. Gibbs. "On the Temperature Dependence of Cooperative Relaxation Properties in Glass-Forming Liquids." *The Journal of Chemical Physics* 43.1 (1965): 139.

Angell, C. A., and Martin Goldstein. *Dynamic Aspects of Structural Change in Liquids and Glasses*. Vol. 484. New York, NY: New York Academy of Sciences, 1986.

Angell, C.A. and D.L. Smith. “Test of the Entropy Basis of the VTF Equation: Dielectric Relaxation of Polyalcohols near Tg.” *Journal of Physical Chemistry*, 86, 3845 (1982).

Bailey, R. T., Alastair M. North, and R. A. Pethrick. *Molecular Motion in High Polymers*. Oxford: Clarendon, 1981.

Barrat, J.L. and Klein, M.L. “Molecular Dynamics Simulations of Supercooled Liquids near the Glass Transition.” *Annual Review of Physical Chemistry*, 42, 23 (1991).

Barrat, J.L., J.N. Roux, and J.P. Hansen. "Diffusion, Viscosity and Structural Slowing down in Soft Sphere Alloys near the Kinetic Glass Transition." *Chemical Physics* 149.1-2 (1990): 197-208.

Bengtzelius, U., W. Gotze, and A. Sjolander. "Dynamics of Supercooled Liquids and the Glass Transition." *Journal of Physics C: Solid State Physics* 17.33 (1984): 5915-934.

Bernu, B., J. Hansen, Y. Hiwatari, and G. Pastore. "Soft-sphere Model for the Glass Transition in Binary Alloys: Pair Structure and Self-diffusion." *Physical Review A*36.10 (1987): 4891-903.

Bicerano, Jozef. *Prediction of Polymer Properties*. New York: Marcel Dekker, 2002.

Böhmer, R., K. L. Ngai, C. A. Angell, and D. J. Plazek. "Nonexponential Relaxations in Strong and Fragile Glass Formers." *The Journal of Chemical Physics* 99.5 (1993): 4201-209.

Boon, Jean-Pierre, and Sidney Yip. *Molecular Hydrodynamics*. New York: Dover Publications, 1991.

Bratsch, Steven G. "Electronegativity Equalization with Pauling Units." *Journal of Chemical Education* 61.7 (1984): 588-89.

Brawer, Steven. *Relaxation in Viscous Liquids and Glasses: Review of Phenomenology, Molecular Dynamics Simulations, and Theoretical Treatment.* Columbus, OH: American Ceramic Society, 1985.

Bueche, F. "Segmental Mobility of Polymers Near Their Glass Temperature." *The Journal of Chemical Physics* 21.10 (1953): 1850.

Cao, C., and Y. Lin. "Correlation between the Glass Transition Temperatures and Repeating Unit Structure for High Molecular Weight Polymers." *Journal of Chemical Information and Modeling* 43.2 (2003): 643-50.

Chenzhong, C., and L. Zhiliang. "Molecular Polarizability. 1. Relationship to Water Solubility of Alkanes and Alcohols." *Journal of Chemical Information and Modeling* 38.1 (1998): 1-7.

Chow, T. S. "Molecular Interpretation of the Glass Transition Temperature of Polymer-Diluent Systems." *Macromolecules* 13.2 (1980): 362-64.

Claudy, P., J. M. LeToffe, Y. Camberlain, and J. P. Pascault. "Glass Transition of Polystyrene versus Molecular Weight." *Polymer Bulletin* 9-9.4-5 (1983): 208-15.

Cowie, J.M.G. "Some General Features of Relations for Oligomers and Amorphous Polymers." *European Polymer Journal* 11.4 (1975): 297-300.

Crompton, T. R. *Thermal Stability of Polymers*. Shrewsbury, U.K.: Smithers Rapra, 2012.

Das, Shankar, Gene Mazenko, Sriram Ramaswamy, and John Toner. "Hydrodynamic Theory of the Glass Transition." *Physical Review Letters* 54.2 (1985): 118-21.

Debenedetti, P. and Stillinger, F. “Supercooled Liquids and the Glass Transition”. *Nature*, 410, 259 (2001).

Dobkowski, Z. "Influence of Molecular Weight Distribution and Long Chain Branching on the Glass Transition Temperature of Polycarbonate." *European Polymer Journal* 18.7 (1982): 563-67.

Dorfmüller, Thomas, and G. Williams. *Molecular Dynamics and Relaxation Phenomena in Glasses: Proceedings of a Workshop Held at the Zentrum Für Interdisziplinäre Forschung Universität Bielefeld, Bielefeld, FRG, November 11-13, 1985*. Vol. 277. Berlin: Springer-Verlag, 1987.

Dudowicz, Jacek, Karl F. Freed, and Jack F. Douglas. "The Glass Transition Temperature of Polymer Melts." *The Journal of Physical Chemistry B* 109.45 (2005): 21285-1292.

Earnest, C. M. “Assignment of Glass Transition Temperatures Using Thermomechanical Analysis,” *Assignment of the Glass Transition*, *ASTM STP 1249*, R. J. Seyler, Ed., American Society for Testing and Materials, Philadelphia, 1994, pp. 75-87.

Ediger, M. D. "Spatially Heterogeneous Dynamics in Supercooled Liquids." *Annual Review of Physical Chemistry* 51.1 (2000): 99-128.

Fedors, R.F. "Glass Transition Temperatures and Molecular Weight." *Polymer* 20.9 (1979): 1055-1056.

Fox, T. G., and P. J. Flory. "Second-Order Transition Temperatures and Related Properties of Polystyrene. Influence of Molecular Weight." *Journal of Applied Physics* 21.6 (1950): 581.

Fox, T. G., and S. Loshaek. "Influence of Molecular Weight and Degree of Crosslinking on the Specific Volume and Glass Temperature of Polymers." *Journal of Polymer Science* 15.80 (1955): 371-90.

Fredrickson, Glenn. "Recent Developments in Dynamical Theories of the Liquid-Glass Transition". *Annual Review of Physical Chemistry*, 39, 149 (1988).

Fredrickson, Glenn, and Hans Andersen. "Kinetic Ising Model of the Glass Transition." *Physical Review Letters* 53.13 (1984): 1244-247.

Fulcher, Gordon S. "Analysis of Recent Measurements of the Viscosity Of Glasses." *Journal of the American Ceramic Society* 8.6 (1925): 339-55.

Gerdeen, James C., and Ronald A. L. Rorrer. *Engineering Design with Polymers and Composites*. Boca Raton, FL: CRC, 2012.

Gibbs, Julian H., and Edmund A. Dimarzio. "Nature of the Glass Transition and the Glassy State." *The Journal of Chemical Physics* 28.3 (1958): 373-83.

Goldstein, Martin, and Robert Simha. *The Glass Transition and the Nature of the Glassy State*. Vol. 279. New York: New York Academy of Sciences, 1976.

Götze, W., and L. Sjögren. "α-relaxation near the Liquid-glass Transition." *Journal of Physics C: Solid State Physics* 20.7 (1987): 879-94.

Gupta, P. and Muaro, J. "The Laboratory Glass Transition". *Journal of Chemical Physics*, 126, 22 (2007).

Haynes, William M. *CRC Handbook of Chemistry and Physics: A Ready-reference Book of Chemical and Physical Data*. Boca Raton, FL.: CRC, 2011.

Hiemenz, Paul C., and Timothy Lodge. *Polymer Chemistry*. Boca Raton: CRC, 2007.

Hopkins, Paul, Andrea Fortini, Andrew J. Archer, and Matthias Schmidt. "The Van Hove Distribution Function for Brownian Hard Spheres: Dynamical Test Particle Theory and Computer Simulations for Bulk Dynamics." *The Journal of Chemical Physics* 133.22 (2010).

Huggins, Maurice L. "Solutions of Long Chain Compounds." *The Journal of Chemical Physics* 9.5 (1941): 440.

Katritzky, A.R., S. Sild, V. Lobanov, and M. Karelson. "Quantitative Structure-Property Relationship (QSPR) Correlation of Glass Transition Temperatures of High Molecular Weight Polymers." *Journal of Chemical Information and Modeling* 38.2 (1998): 300-04.

Kauzmann, Walter. "The Nature of the Glassy State and the Behavior of Liquids at Low Temperatures." *Chemical Reviews* 43.2 (1948): 219-56.

Kim, Yong Woo, Jung Tae Park, Joo Hwan Koh, Byoung Ryul Min, and Jong Hak Kim. "Molecular Thermodynamic Model of the Glass Transition Temperature: Dependence on Molecular Weight." *Polymers for Advanced Technologies* 19.8 (2008): 944-46.

Kunal, K., M. Paluch, C. M. Roland, J. E. Puskas, Y. Chen, and A. P. Sokolov. "Polyisobutylene: A Most Unusual Polymer." *Journal of Polymer Science Part B: Polymer Physics* 46.13 (2008): 1390-399.

Le, Tu, V. Chandana Epa, Frank R. Burden, and David A. Winkler. "Quantitative Structure–Property Relationship Modeling of Diverse Materials Properties." *Chemical Reviews* 112.5 (2012): 2889-919.

Lee, Kyung Ju, Do Kyoung Lee, Yong Woo Kim, Woo-Seok Choe, and Jong Hak Kim. "Theoretical Consideration on the Glass Transition Behavior of Polymer Nanocomposites." *Journal of Polymer Science Part B: Polymer Physics* 45.16 (2007): 2232-238.

Leutheusser, E. "Dynamical Model of the Liquid-glass Transition." *Physical Review A*29.5 (1984): 2765-773.

Lubchenko, Vassiliy, and Peter G. Wolynes. "Theory of Structural Glasses and Supercooled Liquids." *Annual Review of Physical Chemistry* 58.1 (2007): 235-66.

Mark, James E. *Physical Properties of Polymers*. Cambridge: Cambridge UP, 2004.

Más, J., A. Vidaurre, J. M. Meseguer, F. Romero, M. Monleón Pradas, J. L. Gómez Ribelles, M. L. L. Maspoch, O. O. Santana, P. Pagés, and J. Pérez-Folch. "Dynamic Mechanical Properties of Polycarbonate and Acrylonitrile–butadiene–styrene Copolymer Blends." *Journal of Applied Polymer Science* 83.7 (2002): 1507-516.

Meyers, Marc A., and Krishan Kumar Chawla. *Mechanical Behavior of Materials*. Cambridge: Cambridge UP, 2010.

Moynihan, Cornelius T., Allan J. Easteal, James Wilder, and Joseph Tucker. "Dependence of the Glass Transition Temperature on Heating and Cooling Rate." *The Journal of Physical Chemistry* 78.26 (1974): 2673-677.

Ngai, K. L., R. W. Rendell, and D. J. Plazek. "Couplings between the Cooperatively Rearranging Regions of the Adam–Gibbs Theory of Relaxations in Glass-forming Liquids." *The Journal of Chemical Physics* 94.4 (1991): 3018-029.

Ogawa, Toshio. "Effects of Molecular Weight on Mechanical Properties of Polypropylene." *Journal of Applied Polymer Science* 44.10 (1992): 1869-871.

Painter, P. and Coleman, M. *Fundamentals of Polymer Science: an Introductory Text*. Lancaster: Technomic Publishing, 1997.

Palmer, R. G. "Broken Ergodicity." *Advances in Physics* 31.6 (1982): 669-735.

Roland, C. M. “Characteristic Relaxation Times and their Invariance to Thermodynamic Conditions.” *Soft Matter* 4.12 (2008): 2316-22.

Scherer, George W. *Relaxation in Glass and Composites*. Malabar, FL: Krieger Pub., 1992.

Seyler, Rickey J. *Assignment of the Glass Transition*. Philadelphia, PA: ASTM, 1994.

Skoog, Douglas A., F. James. Holler, and Timothy A. Nieman. *Principles of Instrumental Analysis*. Philadelphia: Saunders College Pub., 1998.

Taborek, P., R. Kleiman, and D. Bishop. "Power-law Behavior in the Viscosity of Supercooled Liquids." *Physical Review B* 34.3 (1986): 1835-840.

Van Dijk, Menno A., and André Wakker. *Concepts of Polymer Thermodynamics*. Lancaster: Technomic Pub., 1997.

Van Krevelen, D. W., and K. T. Nijenhuis. *Properties of Polymers: Their Correlation with Chemical Structure: Their Numerical Estimation and Prediction from Additive Group Contributions*. Amsterdam: Elsevier, 2009.

Wang, Junmei, and Tingjun Hou. "Application of Molecular Dynamics Simulations in Molecular Property Prediction II: Diffusion Coefficient." *Journal of Computational Chemistry* 32.16 (2011): 3505-519.

Weber, Thomas, Glenn Fredrickson, and Frank Stillinger. "Relaxation Behavior in a Tiling Model for Glasses." *Physical Review B* 34.11 (1986): 7641-651.

Williams, Graham, and David C. Watts. "Non-symmetrical Dielectric Relaxation Behavior Arising from a Simple Empirical Decay Function." *Transactions of the Faraday Society* 66 (1970): 80-85.

Yu, Xinliang, Wenhao Yu, and Xueye Wang. "A Simple Three-descriptor Model for the Prediction of the Glass-transition Temperatures of Vinyl Polymers." *Journal of Applied Polymer Science* 115.6 (2010): 3721-726.

Appendix A – Glass Transition and Melting Temperatures for Common Polymers (Gerdeen et. al, 2012)

Polymer	Abbreviation	T_g (℃)	T_m (℃)
Polyethylene	PE	-90 to -135	115 to 137
Polypropylene	PP	-10	176
Polystyrene	PS	95	240
Polyvinyl Chloride	PVC	85	212
Polyvinyl Fluoride	PVF	-20 to 45	200
Polyvinylidene Chloride	PVDC	-15	198
Polyamide 6	PA6	50	215
Polyamide 6 / 6	PA6/6	90	260
Poly(methyl methacrylate)	PMMA	105	175
Polycarbonate	PC	150	265
Natural Rubber	NR	-75	28
Poly(acrylonitrile-co-butadiene-co-styrene)	ABS	100	230
Polytetrafluoroethylene	PTFE	-65	327
Butyl Rubber	BR	-90	154
Polyethylene Terephthalate	PET	68 to 80	212 to 265

Appendix B – Parameter Values and Corresponding T_g Values for Select Polymers Using 5-descriptor QSPR Model (Cao & Lin, 2003 and Katritzky et. al, 1998)

Polymer	$\Sigma MV_{ter}(R_{ter})$	L_F	ΔX_{SB}	ΔPEI	$Q_{\pm}$	$T_g(K)_{calc}$	$T_g(K)_{exp}$
Poly(ethylene)	0.0	0	0	0	0	204	195
Poly(ethylethylene)	102.0	1	0	2.2909	0	256	228
Poly(butylethylene)	102.0	3	0	2.4438	0	239	220
Poly(cyclopentylethylene)	282.2	0	0	2.7085	0	339	348
Poly(cyclohexylethylene)	310.5	0	0	2.7683	0	350	363
Poly(acrylic acid)	139.2	0	0.3350	2.0174	-0.0483	380	379
Poly(methyl acrylate)	102.0	2	0.2096	2.1170	0	274	281
Poly(ethyl acrylate)	102.0	3	0.1634	2.1703	0	259	251
Poly(*sec*-butyl acrylate)	102.0	3	0.1245	2.2567	0	255	253
Poly(vinyl alcohol)	77.9	0	0.2737	0.8957	-0.0483	337	358
Poly(vinyl chloride)	93.2	0	0.5126	2.1800	0	331	348
Poly(acrylonitrile)	106.0	0	0.3209	1.9146	-0.0692	388	378
Poly(vinyl acetate)	166.4	1	0.2096	1.2195	0	300	301
Poly(styrene)	275.2	0	0.1050	2.5699	0	349	373
Poly(2-chlorostyrene)	307.8	0	0.1466	2.6427	0	368	392
Poly(3-chlorostyrene)	315.7	0	0.1466	2.6055	0	371	363
Poly(4-chlorostyrene)	309.0	0	0.1466	2.5908	0	368	389
Poly(2-methylstyrene)	323.3	0	0.0958	2.6695	0	368	409
Poly(3-methylstyrene)	327.1	0	0.0958	2.6232	0	369	374
Poly(4-methylstyrene)	319.6	0	0.0958	2.6030	0	366	374
Poly(4-fluorostyrene)	290.4	0	0.1669	2.5684	0	364	379
Poly(propylene)	102.0	0	0	2.0411	0	262	233
Poly(1-pentene)	102.0	2	0	2.3905	0	247	220
Poly(ethoxyethylene)	102.0	2	0.1117	1.2451	0	253	254
Poly(*tert*-butyl acrylate)	258.1	2	0.1245	2.2769	0	325	315
Poly(*n*-butyl acrylate)	102.0	5	0.1245	2.2261	0	236	219
Poly(vinyl hexyl ether)	102.0	6	0.0821	1.3705	0	214	209
Poly(1,1-dimethylethylene)	0	0	0	4.0821	0	241	199
Poly(1,1-dichloroethylene)	0	0	0	4.3600	0	243	256
Poly(1,1-difluoroethylene)	0	0	0	1.1140	0	214	233
Poly(α-methylstyrene)	377.2	0	0.0956	4.6110	0	406	409
Poly(methyl methacrylate)	211.3	2	0.2084	4.1581	0	335	378

Appendix B (continued)

Polymer	$\Sigma MV_{ter}(R_{ter})$	L_F	ΔX_{SB}	ΔPEI	$Q_{\pm}$	$T_g(K)_{calc}$	$T_g(K)_{exp}$
Poly(ethyl methacrylate)	211.3	3	0.1595	4.2114	0	320	324
Poly(isopropyl methacrylate)	258.1	2	0.1336	4.2647	0	344	327
Poly(ethyl chloroacrylate)	195.2	3	0.5175	4.3503	0	364	366
Poly(2-chloroethyl methacrylate)	195.2	4	0.2108	4.2323	0	312	365
Poly(*tert*-butyl methacrylate)	408.0	2	0.1174	4.3180	0	401	380
Poly(phenyl methacrylate)	377.2	2	0.1709	4.2929	0	396	393
Poly(chlorotrifluoroethylene)	162.0	0	0.4322	3.8510	0	362	373
Poly(oxymethylene)	0	0	0	0	0	204	218
Poly(oxyethylene)	0	0	0	0	0	204	206
Poly(oxytrimethylene)	0	0	0	0	0	204	195
Poly(oxytetramethylene)	0	0	0	0	0	204	190
Poly(ethylene terephthalate)	58.0	0	0.7449	0.8020	0	337	345
Poly(vinyl *n*-octyl ether)	102.0	8	0.0776	1.3915	0	196	194
Poly(vinyl *n*-decyl ether)	102.0	10	0.0748	1.4053	0	178	197
Poly(oxyoctamethylene)	0	0	0	0	0	204	203
Poly(oxyhexamethylene)	0	0	0	0	0	204	204
Poly(vinyl *n*-pentyl ether)	102.0	5	0.0855	1.3541	0	223	207
Poly(vinyl 2-ethylhexyl ether)	102.0	6	0.0796	1.4238	0	214	207
Poly(*n*-octyl acrylate)	102.0	9	0.0976	2.2706	0	197	208
Poly(*n*-octyl methylacrylate)	211.3	9	0.0871	4.3117	0	257	253
Poly(*n*-heptyl acrylate)	102.0	8	0.1019	2.2634	0	207	213
Poly(*n*-nonyl acrylate)	102.0	10	0.0942	2.2773	0	188	216
Poly(*n*-hexyl acrylate)	102.0	7	0.1073	2.2550	0	216	216
Poly(1-heptene)	102.0	4	0	2.4768	0	230	220
Poly(vinyl n-butyl ether)	102.0	4	0.0905	1.3315	0	233	221
Poly(*n*-propyl acrylate)	102.0	4	0.1393	2.2034	0	247	229
Poly(vinylisobutyl ether)	211.3	2	0.0905	1.3517	0	293	251
Poly(vinyl *sec*-butyl ether)	102.0	3	0.0905	1.3980	0	242	253
Poly(pentafluoroethyl ethylene)	68.8	2	0.6374	2.2442	0	322	314
Poly(2,3,3,3-tetrafluoropropylene)	137.6	1	0.6712	2.5518	0	365	315
Poly(3,3-dimethylbutyl methacrylate)	408.0	4	0.0751	4.3124	0	377	318
Poly(*n*-butyl acrylamide)	211.3	5	0.1267	4.3411	-0.0257	329	319
Poly(vinyl trifluoroacetate)	68.8	3	0.5793	1.2118	0	295	319

Appendix B (continued)

Polymer	$\Sigma MV_{ter}(R_{ter})$	L_F	ΔX_{SB}	ΔPEI	Q_+	$T_g(K)_{calc}$	$T_g(K)_{exp}$
Poly(3-methyl-1-butene)	211.3	0	0	2.5407	0	309	323
Poly(*n*-butyl α-chloroacrylate)	195.2	5	0.5228	4.4061	0	348	330
Poly(*sec*-butyl methacrylate)	211.3	4	0.1174	4.2978	0	306	330
Poly(heptafluoropropyl ethylene)	68.8	3	0.6268	2.3413	0	312	331
Poly(3-pentyl acrylate)	102.0	4	0.1145	2.2898	0	245	257
Poly(5-methyl-1-hexene)	211.3	2	0	2.4971	0	291	259
Poly(oxy-2,2-dichloromethyltrimethylene)	0	1	0.0083	4.5173	0	237	265
Poly(*n*-hexyl methacrylate)	211.3	7	0.0982	4.2960	0	276	268
Poly(vinyl isopropyl ether)	211.3	1	0.0981	1.3447	0	303	270
Poly[*p*-(*n*-butyl)styrene]	102.0	3	0.0828	2.6546	0	252	279
Poly(*n*-butyl methacrylate)	211.3	5	0.1174	4.2671	0	297	293
Poly(2-methoxyethyl methacrylate)	211.3	5	0.1648	2.2008	0	285	293
Poly(3,3,3-trifluoropropylene)	68.8	1	0.6643	1.9948	0	332	300
Poly(4-methyl-1-pentene)	211.3	1	0	2.4901	0	300	302
Poly(vinyl chloroacetate)	93.2	3	0.2831	1.2551	0	264	304
Poly(*n*-propyl methacrylate)	211.3	4	0.1336	4.2445	0	308	306
Poly(3-cyclopentyl-1-propene)	282.2	1	0	2.5469	0	328	333
Poly(3-phenyl-1-propene)	275.2	1	0	2.5267	0	325	333
Poly(*n*-propyl α-chloroacrylate)	195.2	4	0.5210	4.3834	0	356	344
Poly(*sec*-butyl α-chloroacrylate)	195.2	4	0.5228	4.4367	0	357	347
Poly(3-cyclohexyl-1-propene)	310.5	1	0	2.5832	0	340	348
Poly(vinyl acetal)	310.5	1	0.1810	2.0150	0	360	355
Poly(vinyl formal)	310.5	0	0.2589	1.9154	0	378	378

Appendix C – Molecular Descriptor and Corresponding T_g Values for Select Polymers Using 3-descriptor QSPR Model (Yu, Yu, & Wang, 2009)

Polymers	*Mv*	*BIC5*	*Mor13m*	T_g, (exp)	T_g, (calc)[a]	T_g, (calc)[b]
poly(acrylic acid)	0.58	0.276	-0.007	379	378	401
poly(3-thiabutyl acrylate)	0.58	0.852	-0.063	213	227	244
poly(2-chlorophenyl acrylate)	0.69	0.904	-0.496	326	327	330
poly(2,4-dichlorophenyl acrylate)	0.73	0.904	-0.264	333	340	345
poly(2-cyanoisobutyl acrylate)	0.59	0.725	-0.221	324	303	295
poly(2-cyanoethyl acrylate)	0.61	0.826	-0.114	277	273	275
poly(5-cyano-3-oxapentyl acrylate)	0.59	0.870	-0.291	250	241	258
poly(2-cyanoisopropyl acrylate)	0.60	0.659	-0.222	339	320	320
poly(4-biphenyl acrylate)	0.68	0.807	-0.877	383	387	371
poly(dodecyl acrylate)	0.54	0.806	-0.384	270	259	246
poly(2-ethoxyl-carbonyl-phenyl acrylate)	0.63	0.883	-0.288	303	282	283
poly(2-ethoxyethyl acrylate)	0.55	0.858	-0.285	223	233	234
poly(ethyl acrylate)	0.55	0.862	-0.274	249	231	232
poly(4-butoxycarbonylphenyl acrylate)	0.61	0.841	-0.506	286	298	292
poly(1H,1H-heptafluorobutyl acrylate)	0.59	0.849	0.176	243	227	239
poly(2,2,3,3,5,5,5-heptafluoro-4-oxapentyl acrylate)	0.59	0.858	0.426	218	223	223
poly(heptyl acrylate)	0.55	0.864	-0.245	213	229	230
poly(hexadecyl acrylate)	0.54	0.695	-0.511	308	311	284
poly(hexyl acrylate)	0.55	0.860	-0.207	216	227	229
poly(isobutyl acrylate)	0.55	0.728	-0.185	249	254	264
poly(6-cyano-4-thiahexyl acrylate)	0.60	0.873	-0.162	215	238	258
poly(2-methoxycarbonylphenyl acrylate)	0.64	0.883	-0.332	319	299	292
poly(4-methoxycarbonylphenyl acrylate)	0.64	0.818	-0.418	340	318	315
poly(4-methoxyphenyll acrylate)	0.63	0.808	-0.645	324	326	323

Appendix C (continued)

Polymers	*Mv*	*BIC5*	*Mor13m*	T_g, (exp)	T_g, (calc)[a]	T_g, (calc)[b]
poly(*sec*-butyl acrylate)	0.55	0.818	-0.146	250	228	237
poly(2-methylbutyl acrylate)	0.55	0.848	-0.200	241	227	232
poly(2-methyl-7-ethyl-4-undecyl acrylate)	0.54	0.833	-0.406	253	257	240
poly(2-naphthyl acrylate)	0.68	0.885	-0.752	358	341	342
poly(1H,1H-nonafluoro-4-oxahexyl acrylate)	0.59	0.862	0.920	224	223	195
poly(nonyl acrylate)	0.54	0.871	-0.294	215	232	223
poly(1h,1h,5h-octafluoropentyl acrylate)	0.59	0.880	0.094	238	223	235
poly(pentachlorophenyl acrylate)	0.84	0.812	0.702	420	413	395
poly(*n*-pentyl acrylate)	0.55	0.855	-0.193	216	226	229
polyphenylethyl acrylate)	0.62	0.832	-0.423	270	303	297
poly(phenyl acrylate)	0.65	0.812	-0.507	330	325	328
poly(tetradecyl acrylate)	0.54	0.748	-0.443	297	288	266
poly(4,4,5,5-tetrafluoro-3-oxapentyl acrylate)	0.57	0.885	-0.075	251	222	228
poly(4-tertbutylphenyl acrylate)	0.61	0.688	-0.655	344	342	343
poly(o-totyl acrylate)	0.64	0.873	-0.517	325	311	305
poly(2,2,2trifluoroethyl acrylate)	0.57	0.813	-0.076	263	231	249
poly(3,3,5-trimethylcyclohexyl acrylate)	0.56	0.812	-0.481	288	278	264
poly(1H,1H-undecafluorohexyl acrylate)	0.59	0.860	-0.014	234	228	246
poly(5-cyano-3-thiapentyl acrylate)	0.61	0.870	-0.025	223	243	258
poly(3-chloro-2,2-bis(chloromethyl)propyl acrylate)	0.64	0.702	-0.198	319	325	335
poly(4-chlorophenyl acrylate)	0.69	0.812	-0.403	331	340	350
poly(4-cyanobenyl acrylate)	0.67	0.816	-0.425	317	329	337
poly(4-cyanobutyl acrylate)	0.59	0.862	-0.177	233	235	254
poly(4-thiapentyl acrylate)	0.58	0.858	-0.085	208	227	244
poly(benzyl acrylate)	0.64	0.823	-0.441	279	318	315
poly(4-cyanophenyl acrylate)	0.69	0.804	-0.557	363	354	361

Appendix C (continued)

Polymers	*Mv*	*BIC5*	*Mor13m*	T_g, (exp)	T_g, (calc)[a]	T_g, (calc)[b]
poly(3-dimethylaminophenyl acrylate)	0.61	0.806	-0.831	320	337	320
poly(4-ethoxyl-carbonyl-phenyl acrylate)	0.63	0.827	-0.460	310	314	308
poly(3-ethoxyl-carbonyl-phenyl acrylate)	0.63	0.883	-0.504	297	299	294
poly(3-ethoxypropyl acrylate)	0.55	0.862	-0.274	218	231	232
poly(2-ethylbutyl acrylate)	0.55	0.746	-0.195	223	249	260
poly(fluoromethyl acrylate)	0.58	0.676	-0.143	288	307	297
poly(5,5,6,6,7,7,7-heptafluoro-3-oxaheptyl acrylate)	0.57	0.866	-0.220	228	229	242
poly(heptafluoro-2-propyl acrylate)	0.60	0.655	0.471	283	315	284
poly(2-heptyl acrylate)	0.55	0.859	-0.193	235	226	228
poly(butyl acrylate)	0.55	0.849	-0.152	219	225	229
poly(isopropyl acrylate)	0.56	0.655	-0.127	270	295	288
poly(3-methoxybutyl acrylate)	0.55	0.856	-0.299	217	234	235
poly(3-methoxycarbonylphenyl acrylate)	0.64	0.883	-0.431	311	304	297
poly(2-methoxyethyl acrylate)	0.55	0.852	-0.254	223	231	233
poly(3-methoxypropyl acrylate)	0.55	0.858	-0.226	198	228	230
poly(methyl acrylate)	0.57	0.583	-0.068	283	317	312
poly(3-methylbutyl acrylate)	0.55	0.776	-0.183	228	238	251
poly(2-methylpentyl acrylate)	0.55	0.854	-0.231	235	229	232
poly(neopentyl acrylate)	0.55	0.625	-0.175	295	301	292
poly(1H,1H-nonafluoropentyl acrylate)	0.59	0.855	0.336	236	224	228
poly(*tert*-butyl acrylate)	0.55	0.536	-0.317	304	324	325
poly(1H,1H-pentafluoropropyl acrylate)	0.59	0.813	0.133	247	238	251
poly(3-pentyl acrylate)	0.55	0.698	-0.157	267	265	271
poly(2-tertbutylphenyl acrylate)	0.61	0.738	-0.713	345	337	332
poly(propyl acrylate)	0.56	0.813	-0.135	236	230	245
poly(7,7,8,8-tetrafluoro-3,6-dioxaoctyl acrylate)	0.56	0.892	-0.169	233	223	225

Appendix C (continued)

Polymers	*Mv*	*BIC5*	*Mor13m*	T_g, (exp)	T_g, (calc)[a]	T_g, (calc)[b]
poly(5-thiahexyl acrylate)	0.57	0.862	-0.078	203	223	235
poly(m-totyl acrylate)	0.64	0.873	-0.530	298	312	306
poly(p-totyl acrylate)	0.64	0.797	-0.547	316	326	328
poly(5,5,5-trifluoro-3-oxapentyl acrylate)	0.57	0.858	-0.191	235	228	242
poly(1H,1H-tridecafluoro-4-oxaoctyl acrylate)	0.59	0.870	0.083	205	224	238
poly(8-cyano-7-thiaoctyl acrylate)	0.59	0.877	0.023	214	225	239
poly(4-thiahexyl acrylate)	0.57	0.862	-0.043	197	223	233
poly(3-thiapentyl acrylate)	0.58	0.858	0.003	202	224	239
poly(vinyl formate)	0.58	0.452	-0.025	304	329	353
poly(4-cyclohexyl-1butene)	0.55	0.784	-0.437	313	277	262
poly(vinyl trifluoroacetate)	0.60	0.654	0.294	319	315	294
poly(3-methyl-1-butene)	0.53	0.208	-0.180	323	361	395
poly(3-phenyl-1propene)	0.63	0.799	-0.440	333	318	314
poly(vinyl *n*-octyl ether)	0.53	0.865	-0.301	194	234	218
poly(vinyl *n*-pentyl ether)	0.53	0.850	-0.208	207	227	218
poly(vinyl *n*-hexyl ether)	0.53	0.856	-0.235	209	229	217
poly(1-hexene)	0.53	0.768	-0.147	223	233	237
poly(1-heptene)	0.53	0.816	-0.160	220	227	224
poly(vinyl *sec*-butyl ether)	0.53	0.775	-0.328	253	256	245
poly(vinyl ethyl ether)	0.53	0.661	-0.167	254	275	268
poly(vinyl chloroacetate)	0.63	0.737	0.048	304	317	305
poly(5-methyl-hexene)	0.53	0.685	-0.147	259	260	260
poly(6-methyl-heptene)	0.53	0.745	-0.198	239	244	246
poly(vinyl isobutyral)	0.56	0.377	-0.169	329	342	368
poly(vinyl propional)	0.56	0.472	-0.120	345	324	339
poly(vinyl acetal)	0.57	0.418	-0.088	355	333	359
poly(vinyl *n*-butyl ether)	0.53	0.815	-0.187	221	229	226
poly(vinyl acetate)	0.57	0.654	-0.055	301	302	292
poly(4-methyl-1-pentene)	0.53	0.528	-0.128	302	315	303

[a] T_g values calculated with the ANN model. [b] T_g values calculated with the MLR model.